Desalination and Water Treatment
www.deswater.com
doi: 10.5004/dwt.2022.28506

261 (2022) 195–213
June

Watermelon peels biochar-S for adsorption of Cu^{2+} from water

Mohamed A. El-Nemr[a], Murat Yılmaz[b], Safaa Ragab[c], Ahmed El Nemr[c,*]

[a]*Department of Chemical Engineering, Faculty of Engineering, Minia University, Minia, Egypt, email: mohamedelnemr1992@yahoo.com (M.A. El-Nemr)*
[b]*Department of Chemical Engineering, Faculty of Engineering, Osmaniye Korkut Ata University, 80000 Osmaniye, Turkey, email: muratyilmaz@osmaniye.edu.tr (M. Yılmaz)*
[c]*Environment Division, National Institute of Oceanography and Fisheries (NIOF), Kayet Bey, Elanfoushy, Alexandria, Egypt, emails: ahmedmoustafaelnemr@yahoo.com/ahmed.m.elnemr@gmail.com (A. El Nemr), safaa_ragab65@yahoo.com (S. Ragab)*

Received 27 November 2021; Accepted 16 April 2022

ABSTRACT

In this study, new biochar was produced from watermelon peel residues by dehydration process. The ability of the newly generated biochar-S to remove Cu^{2+} ions from aqueous solutions was examined. Watermelon peel was used to make biochar-S, which was made by dehydrating by boiling with 50% sulfuric acid. Scanning electron microscopy, Brunauer–Emmett–Teller, Fourier-transform infrared spectroscopy, Barrett–Joyner–Halenda, differential scanning calorimetry, thermal gravimetric analysis and energy-dispersive X-ray analysis studies were used to characterize the biochar-S. The ideal pH for Cu^{2+} ion adsorption was found to be 5.6. 1.0 g L^{-1} of biochar-S as an adsorbents dosage with Cu^{2+} ions beginning concentration of 200 mg L^{-1} had the maximum Cu^{2+} ions removal percentage of 78.33%. The maximal adsorption capacity (Q_m) of biochar-S was 151.52 mg g^{-1}. Isotherm models such as Dubinin–Radushkevich, Langmuir, Temkin, and Freundlich were used to analyze the experimental data. Furthermore, the data of these isotherm models were investigated using several error function equations (average percentage errors, hybrid error function, Chi-square error (χ^2), sum of absolute errors, root mean square errors, and Marquardt's percentage standard deviation). The biochar-S experimental data was best suited by the Freundlich isotherm model. Pseudo-first-order, pseudo-second-order, Elovich, and intraparticle diffusion models were used to assess the kinetic data. The adsorption rate was predominantly influenced by a pseudo-second-order rate model that had a high correlation ($R^2 > 0.99$). The primary mechanism of Cu^{2+} ion adsorption by biochar-S consists mostly of surface precipitation by the formation of insoluble copper compounds in an alkaline state and ion exchange with exchangeable cations in biochar such as aluminium, silicon, and calcium ions for copper ions. The findings suggest that biochar-S is a promising adsorbent for the adsorption of Cu^{2+} ions and that it can be employed repeatedly without losing adsorption efficiency.

Keywords: Biochar; Watermelon peels; Copper removal; Biochar-S; Dehydrated biochar

1. Introduction

Heavy metals are dangerous and naturally occurring substances that can be found in trace levels in water, such as copper, lead, cadmium and mercury [1–3]. Heavy metals released into the environment with the development of industry, agriculture and urbanization threaten human health and the ecosystem [4]. Metallic wastewater is generated as a result of industrial activities such as mining, metallurgy, electroplating, alloy production and galvanization of iron products. This water serves as a potential source for the recovery of precious metals [5,6]. The typical characteristics

* Corresponding author.

of metallic wastewater can be listed as low chemical oxygen demand, low pH and high concentration of heavy metals [7,8]. Governments strictly control the discharge of heavy metals into watersheds and drinking water sources, making legal standards on environmental control stringent [9]. Therefore, it is of great importance to treat heavy metals before they are discharged into the environment [10–12]. Copper, mercury, nickel, cadmium, zinc, lead, and chromium are just a few of the heavy metals that are known to pose a significant threat to human health, water quality, and biodiversity in the ecosystem. Copper, mercury, nickel, cadmium, zinc, lead, and chromium are also known to pose a significant threat to human health, water quality, and biodiversity in the ecosystem [9,13]. Among these metals, extensive research has been done on copper metal. Studies conducted in the last decade have shown that copper ions in wastewater cause the development of cardiovascular diseases, diabetes and several diseases [14].

There are many techniques such as ultrafiltration, reverse osmosis, precipitation, ion exchange, electrodialysis and phytoextraction to eliminate heavy metals from wastewater. However, these techniques have disadvantages such as being inefficient in waste removal, being expensive, or not being used on a large scale [15,16]. In order to properly dispose of industrial toxic sludge from water bodies, it is critical to identify ecologically benign and economically feasible treatment procedures. The adsorption process is the most widely used wastewater treatment technology for the degradation of heavy metals and dyes, and it is also the most expensive [17–23].

Adsorption is a widely frequent method of wastewater treatment because it is a cost-effective method that successfully eliminates inorganic and organic micro-pollutants from the wastewater [24,25]. Adsorption being an effective method depends on the adsorbent material used in the process. Most scientists working in wastewater treatment use activated carbon, mesoporous carbon, biochar, carbon aerogel, or graphene as adsorbents [26–29].

Studies on the comparison of activated carbon [30–32] and biochar [33–35] have reported that both have high removal efficiency with less modification and cost. Both biochar and activated carbon are obtained from the pyrolysis of waste biomass residues in environments [36–39]. Activated carbon is obtained at relatively higher temperatures compared to biochar, and as a result of the applied activation procedure, it has a higher surface area, more porosity, but fewer surface functional groups [40–42]. Biochar, as opposed to activated carbon, binds effectively to water contaminants because it has a non-carbonized component as well as carboxyl, phenolic, and hydroxyl surface functional groups that contain oxygen [23,27–29,43]. Biochars with rich functional groups such as oxygen, nitrogen and sulfur are used as cheap carbon-based adsorbents in the adsorption of heavy metals or organic pollutants [44–47]. Generally, four different modification methods are used to improve the adsorption capacity of biochar: mineral impregnation, reduction of biochar surface, nanoscale formation and oxidation [48]. The activation of the biochar to be obtained by using suitable raw materials allows it to have a porous structure that allows for remarkable adsorption capacities [23,27–29]. The methods used to prepare activated carbon are divided into two as chemical activation and physical activation. The process of carbonization of raw material at high temperatures under an atmosphere of carbon dioxide (CO_2) or water vapor is called physical activation. The process of reacting the raw material with chemicals such as $ZnCl_2$, KOH, H_2SO_4, HNO_3 and H_3PO_4 at high temperatures in an inert environment is called chemical activation. Many studies have reported in their reports that chemical activation is more advantageous than physical activation [49–54].

Studies conducted in recent years have led to the fact that agricultural wastes and industrial by-products are more preferred than activated carbon in the adsorption process due to their low cost. Fruit peel waste is commonly produced in households and food processing industries. Since they are produced as a by-product in food processing industries, their amount is high, while the amount of domestic waste is very low. With the right processing methods, these wastes, which cause major problems in municipal landfills due to their high biodegradability, can be used as a cheap biosorbent. As a result, not only will these wastes be eliminated from the environment, but they will also earn value as a result of their utilization in a great number of possible applications [55].

Many agricultural wastes have been used as potential and cheap adsorbent material in studies on heavy metal ion removal. Orange peel [56], banana peel [57], citrus peel [58] and mango peel [59] can be given as examples of fruit peels that are frequently used to remove heavy metals from aqueous solutions. Watermelon peels can be included in this group due to the lignocellulose materials in its structure and the carboxylic groups in its shells in removing metal ions from an aqueous solution [60]. Watermelon peels are employed specifically because they produce more waste than other fruit peels due to the size of the watermelons [28,29].

In this study, biochar-S produced from watermelon peels, which is a low-cost agricultural waste material, by dehydration process via boiling in 50% H_2SO_4 was investigated for its efficiency in Cu^{2+} ions removal from aqueous environment. As removal conditions for Cu^{2+} ions from aqueous solution, the effects of pH, starting adsorbent concentration, adsorbent dose, and contact duration between adsorbate and adsorbent were examined. The structure of adsorption and its maximum adsorption capacity was further examined using adsorption isotherms and kinetics of Cu^{2+} ions on biochar-S adsorbent.

2. Materials and methods

2.1. Instrument and materials

The watermelon peel which was used as raw material to obtain biochar-S, an adsorbent material, were obtained from a local market in Alexandria. Sulfuric acid (H_2SO_4, Assay 99%) was supplied from Sigma-Aldrich Company. The standard stock of copper(II) was made from copper sulfate pentahydrate ($CuSO_4{\cdot}5H_2O$) of Sigma-Aldrich. The sodium salt of diethyldithiocarbamate was bought from Loba Chemie, India. Analytik Jena (SPEKOL 1300 UV/Visible Spectrophotometer as a digital spectrophotometer was used with 1 cm optical path glass cells for Cu^{2+} ions concentration

measurements, a shaker (JSOS-500) for mixing operations and a pH meter (JENCO 6173) for pH surveys.

2.2. Methods

2.2.1. Watermelon-biochar preparation

In the synthesis of biochar, watermelon peels obtained from a local market and turned into compost were used as the carbonaceous precursor substance. To eliminate dust from the peels, they were thoroughly cleaned with faucet water many times and then dried in a furnace at 105°C for 72 h before being milled and crushed. A total of 50 g of powdered watermelon peels were heated at 150°C in 200 mL of 50% H_2SO_4 solution for 2 h, then filtered and then washed with pure water until pH 7. Afterward, the samples washed with ethanol were dried in a furnace at 70°C. As a result of this reaction, biochar was generated, which was designated as biochar-S.

2.3. Biochar-S adsorbent characterization

The adsorption–desorption isotherm of biochar-S was carried out in N_2 atmosphere based on a thermodynamic model. Biochar-S surface area was calculated by N_2 adsorption at 77 K with the aid of a surface area and pore analyzer (BELSORP – Mini II, BEL Japan, Inc.) [61,62]. Surface area (S_{BET}) ($m^2\ g^{-1}$), monolayer volume (V_m) (cm^3 (STP)), average pore diameter (MPD) (nm), total pore volume (p_0/p_0) ($cm^3\ g^{-1}$) and energy constant (C) values of biochar-S were calculated using this graph. The mesoporous surface area (S_{mes}), microporous surface area (S_{mi}), mesoporous

Table 1
Isotherm models, kinetic models and errors analysis models [68]

Model name	Equation	
Langmuir	$\frac{C_e}{q_e}=\frac{1}{K_aQ_m}+\frac{1}{Q_m}C_e$	(2)
Freundlich	$\log q_e=\log K_F+\frac{1}{n}\log C_e$	(3)
Temkin	$q_e=B_T\ln A_T+B_T\ln C_e$	(4)
Dubinin–Radushkevich	$\ln q_e=\ln Q_m-K\varepsilon^2$	(5)
	$\varepsilon=RT\ln\left(1+\frac{1}{C_e}\right)$	(6)
Pseudo-first-order	$\log\left(q_e-q_t\right)=\log q_e-\frac{k_1}{2.303}t$	(7)
Pseudo-second-order	$\left(\frac{t}{q_t}\right)=\frac{1}{k_2q_e^2}+\frac{1}{q_e}t$	(8)
Elovich	$q_t=\frac{1}{\beta}\ln\left(\alpha\beta\right)+\frac{1}{\beta}\ln\left(t\right)$	(9)
Intraparticle diffusion	$q_t=K_{dif}t^{1/2}+C$	(10)
APE	$\mathrm{APE}(\%)=\frac{100}{N}\sum_{i=1}^{N}\left\lvert\frac{q_{e,\mathrm{isotherm}}-q_{e,\mathrm{calc}}}{q_{e,\mathrm{isotherm}}}\right\rvert_i$	(11)
HYBRID	$\mathrm{HYBRID}=\frac{100}{N-P}\sum_{i=1}^{N}\left\lvert\frac{q_{e,\mathrm{isotherm}}-q_{e,\mathrm{calc}}}{q_{e,\mathrm{isotherm}}}\right\rvert_i$	(12)
Chi-square	$\chi^2=\sum_{i=1}^{N}\frac{\left(q_{e,\mathrm{isotherm}}-q_{e,\mathrm{calc}}\right)^2}{q_{e,\mathrm{isotherm}}}$	(13)
MPSD	$\mathrm{MPSD}=100\sqrt{\frac{100}{N-P}\sum_{i=1}^{N}\left(\frac{q_{e,\mathrm{calc}}-q_{e,\mathrm{isotherm}}}{q_{e,\mathrm{isotherm}}}\right)_i^2}$	(14)
EABS	$\mathrm{EABS}=\sum_{i=1}^{N}\left\lvert q_{e,\mathrm{calc}}-q_{e,\mathrm{isotherm}}\right\rvert_i$	(15)
RMS	$\mathrm{RMS}=100\sqrt{\frac{1}{N}\sum_{i=1}^{N}\left(1-\frac{q_{e,\mathrm{calc}}}{q_{e,\mathrm{isotherm}}}\right)^2}$	(16)

volume (V_{mes}), and microporous volume (V_{mi}) of biochar-S were evaluated using the Barrett–Joyner–Halenda (BJH) method. The BELSORP analysis program software was used to perform the calculations. The pore-size dispersion was also determined from the desorption isotherm using the BJH technique [63]. With the help of a scanning electron microscope (SEM), the shape of the biochar surface was investigated (QUANTA 250). The functional groups on the surface of biochar-S were studied using Fourier-transform infrared (FTIR) spectroscopy (VERTEX70) and ATR unit model V-100. Using FTIR spectroscopy in conjunction with the platinum ATR unit, IR-observable functional groups on the biochar-S surface were detected in the wavenumber range of 400–4,000 cm^{-1}. Thermal analyzes were carried out using the SDT650-simultaneous thermal analyzer device at a temperature range of 50–1,000°C and a ramped temperature of 5°C min^{-1}.

2.4. Batch adsorption experiment

The sorption capacity, thermodynamic, and kinetic characteristics of biochar-S were determined using a batch experiment adsorption. Number of flasks containing 100 mL of Cu^{2+} solutions of different initial concentrations and biochar-S of varying weights were shaken at 200 rpm for a specific time. Solution pHs were adjusted to desired values using 0.1 M NaOH or HCl. In addition, the pH of the solution was kept fixed at the desired value during the adsorption equilibrium studies. The measurement of the Cu^{2+} concentration was carried out by taking a 0.1 mL sample (separated from the adsorbent) from the solution at regular intervals. The concentration of Cu^{2+} ions was measured using diethyldithiocarbamate as a reagent using a spectrophotometer set at λ_{max} = 460 nm. Eq. (1) was used to determine the adsorption capabilities of adsorbents at time *t*.

$$q_t = \frac{\left(C_0 - C_t\right)}{W} V \tag{1}$$

where C_0 (mg L^{-1}) is the initial concentration of Cu^{2+}; C_t (mg L^{-1}) is the residual concentration of Cu^{2+} at the end of time *t*; q_t (mg g^{-1}) is the adsorption capacity of the adsorbent at time *t*; *W* (g) is the mass of the adsorbent and *V* (L) is the volume of the solution of Cu^{2+} ions.

To examine the effect of pH on the removal of Cu^{2+} ions using biochar-S, studies were achieved at different pH values (2.3 to 6.1) by adding 0.1 g biochar-S to 100 mL of solutions containing 200 ppm Cu^{2+} ions. To modify the pH of the solution, 0.1 M NaOH or HCl solutions were utilized. The shaking process of the mixtures at room temperature at 200 rpm lasted for 20 min, and samples were taken at different intervals for Cu^{2+} ion concentration measurement.

Cu^{2+} solutions at various initial concentrations (50–300 mg L^{-1}) were prepared and the effect of biochar-S dosage on the adsorption of Cu^{2+} ions and isotherm studies were carried out. Cu^{2+} concentrations were measured at intervals in mixtures of 1 to 4 g L^{-1} biochar-S and Cu^{2+} solutions of varied beginning concentrations, which were agitated at 200 rpm at 25°C. All adsorption studies were done in triplicate, and the data are given as a mean.

2.5. Theoretical background

The Langmuir isotherm model [64] posits that adsorption on a surface occurs in a monolayer and that there is no adsorbate migration along the surface's plane [65]. Eq. (2) shows the linear form of the Langmuir equation [66–68], where q_e (mg g^{-1}) expresses the equilibrium adsorption capacities; C_e (mg L^{-1}) expresses the equilibrium concentration; Q_m (mg g^{-1}) expresses the monolayer's maximum adsorption capacity, and K_a (L mg^{-1}) express the equilibrium adsorption sorption energy. The Freundlich model [69] has a linear form, as seen in Eq. (3). The relative adsorption capacity is expressed in K_F; and $1/n$ denotes surface heterogeneity or adsorption density, which becomes more heterogeneous as it approaches zero. Eq. (4) represents the linear form of the Temkin isotherm equation [68,70–74]. It is calculated with $B_T = (RT)/b$ in this equation, *b* is proportional to the heat of adsorption, with the equilibrium binding constant A_T (L mg^{-1}) equal to the maximum binding energy, with the absolute temperature *T* (K), and the universal gas constant *R* (8.314 J mol^{-1} K^{-1}) [75,76]. The Dubinin–Radushkevich model [77–79] is used to evaluate the apparent free energy of porosity and the adsorption characteristic. The Dubinin–Radushkevich isotherm does not make any assumptions about the surface being homogeneous or about the sorption potential being constant. The Dubinin–Radushkevich model has generally been applied in the following linear Eqs. (5) and (6).

The equation written in Eq. (7) [80] is a typical Lagergren first-order model equation, and the adsorption capacity at time *t* (min) is expressed as q_t (mg g^{-1}) and the pseudo-first-order adsorption rate constant k_1 (L min^{-1}). The plot of $\log(q_e - q_t)$ vs. time should yield a linear relationship from which the slope and intercept of the plot, respectively, may be used to derive k_1 and anticipated q_e. Eq. (8) was defined by Ho et al. [81] as a linear pseudo-second-order model, and k_2 (g mg^{-1} min^{-1}) expressed in this model represents the pseudo-second-order adsorption rate constant used to evaluate the initial sorption rate (*h*), *h* is equal to $k_2 q_e^2$. The intercept and slope of the t/q_t against *t* plots, respectively, can be used to determine the values of k_2 and q_e. Eq. (9) shows the linear Elovich kinetic model and the initial adsorption rate is denoted as α (mg g^{-1} min^{-1}) and the desorption constant is denoted by β (g mg^{-1}). The $(1/\beta)\ln(\alpha\beta)$ and $(1/\beta)$ in the model are evaluated from the intercept and slope of the graph between q_t and $\ln(t)$, respectively [82–84]. Using Eq. (10) [85,86], we investigate the potential of intra-particular diffusion. As the intercept *C* value grows, the resistance to external mass transfer rises as well. K_{dif} (mg g^{-1} $min^{-1/2}$) expresses the intraparticle diffusion rate constant, which can be determined directly from the slope of the regression line plotting q_t vs $t^{1/2}$.

Mean percentage error (APE) expressed by Eq. (11) is an equation that specifies the agreement between the experimental and expected data obtained from the isotherm model curves [87]. Eq. (12) [88,89] represents the hybrid fractional error function. Eq. (13) provides the Chi-square error, χ^2 [89]. The following Eq. (14) expresses Marquardt's

percentage standard deviation (MPSD) [87]. The following Eq. (15) provides the total of the absolute errors (EABS) [87]. The following Eq. (16) calculates the root mean square errors (RMS) [87].

3. Results and discussion

3.1. Biochar-S characterization

FTIR spectroscopy was used to detect which functional groups were on the surface of the produced biochar-S adsorbent. As illustrated in Fig. 1, the FTIR graph of the raw watermelon peel was compared to the FTIR graph of the watermelon biochar (Biochar-S). The samples' FTIR spectra reveal alterations in their functional groups. The band between 3,274 and 3,063 cm^{-1} corresponds to stretching oscillation of the O–H found in the watermelon peels and biochar-S (Fig. 1). The large absorption peak near 2,916 cm^{-1} is suggestive of the presence of $–CH_2$ stretching groups in watermelon peels, which were not present in biochar-S (Fig. 1). The strong absorption peak at 1,739.6 cm^{-1} is attributed to the C=O stretching of ester groups in watermelon peels and was converted to a band at 1,701 cm^{-1} as a carboxyl group in biochar-S (Fig. 1). However, when biochar-S was compared to raw watermelon peel, the strength at 1,702.9 cm^{-1} was raised, demonstrating that the carbonyl (C=O) functional group may be augmented by sulphoric acid treatment. The bands at 1,595 cm^{-1} imply the C=O stretching oscillation of β-ketone almost existed in watermelon peel and shifted to 1,589 cm^{-1} in biochar-S, which may also represent to stretching vibration of –C=C- biochar-S (Fig. 1). The peak at 1,402 cm^{-1} represents the C–O functional group in the watermelon peel, which was replaced by the band at 1,413.7 cm^{-1} in biochar-S presented the sulfonyl group (S=O) stretching vibration (Fig. 1). Also, the dehydration with H_2SO_4 led to the formation of a new peak that appeared at 1,153.3 and 1,029.9 cm^{-1} which are due to the formation of sulfonic acid and sulfoxide groups in biochar-S. These new peaks demonstrate the production of the biochar-S as a result of watermelon peels being treated with H_2SO_4. The increase in the –C–O–C– asymmetric stretching functional group, which was partially weak for biochar-S, was more pronounced for watermelon skins, and the presence of oxygenated carbon chains peaked at 1,026 cm^{-1}.

The N_2 adsorption–desorption isotherms of the biochar-S produced were examined to determine the effect of H_2SO_4 on the surface properties of the biochar-S. The Brunauer–Emmett–Teller (BET) and BJH techniques were used to compute the specific surface area and mesopore area, respectively. The textural parameters of biochar-S such as BET specific surface area, mesopore area, mesopore volume, total pore volume, average pore diameter, mesopore distribution peak and monolayer volume are illustrated in Fig. 2. The BET-specific surface area of the biochar-S was 2.42 $m^2\ g^{-1}$, which is very small. The monolayer volume value of biochar-S was 0.56 cm^3 (STP) g^{-1}. The total volume values of biochar-S was 0.008 $cm^3\ g^{-1}$. The mean pore diameters of biochar-S were 14.27 nm. The mesopore surface area, mesopore volume and mesopore distribution peak values of biochar-S were determined as 3.14 $m^2\ g^{-1}$, 0.009 $cm^3\ g^{-1}$ and 1.66 nm, respectively.

Fig. 3 illustrates SEM images of raw watermelon peels and biochar-S. As illustrated in Fig. 3b, biochar-S appears to be clean and devoid of contaminants, and there was no damage to the pore structure of the watermelon peels following treatment with hot sulfuric acid.

Scattered X-ray spectrometry (EDX) was applied to study the chemical composition of biochar-S adsorbent and the percentage of the element is reported in Table 2, which shows the presence of about 32.9% and 14.58% sulfur and oxygen, respectively beside the carbon in 47.12%.

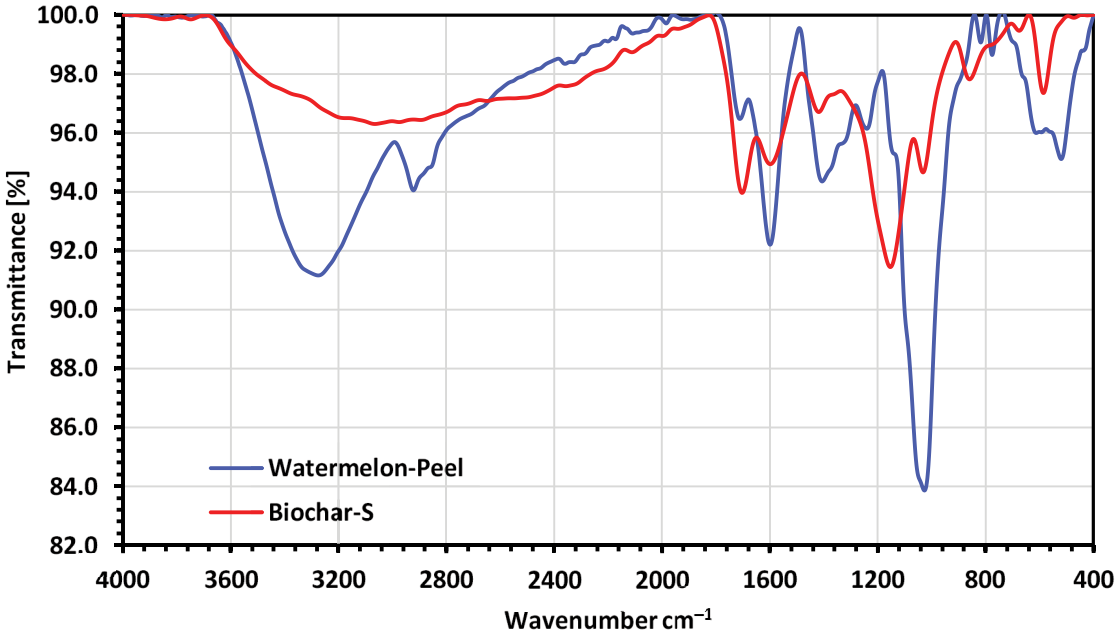

Fig. 1. FTIR analysis of raw watermelon peel and its biochar-S.

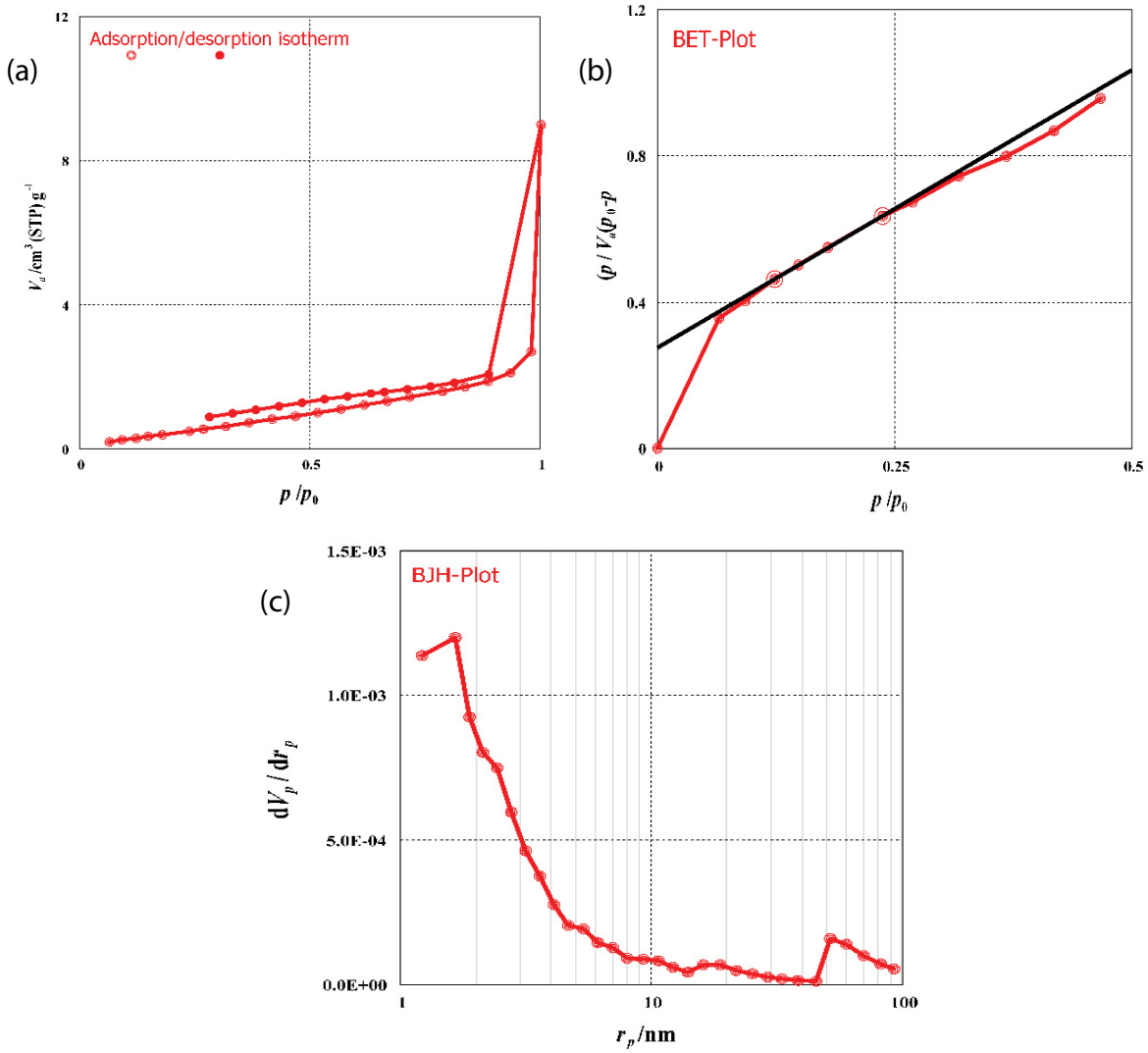

Fig. 2. Graph of (a) N_2 adsorption–desorption, (b) BET analysis, and (c) BJH analysis plot of the biochar-S.

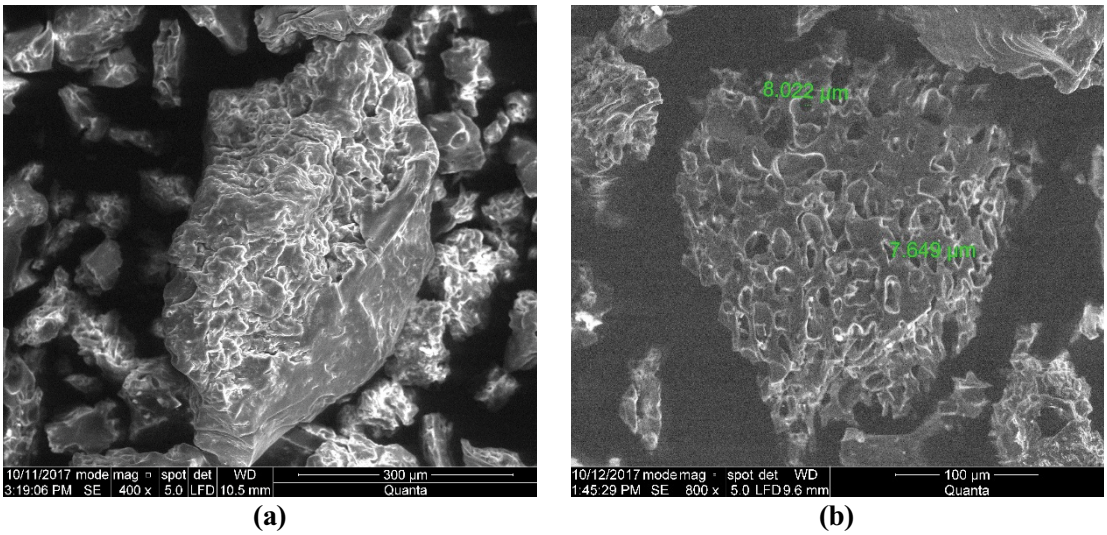

Fig. 3. SEM image of (a) watermelon-peels and (b) biochar-S.

Table 2
Energy-dispersive X-ray analysis data of biochar-S

Biochar	Biochar-S	
Elements	wt.%	at.%
C	47.12	64.80
O	14.58	15.01
S	32.9	16.90
K	3.79	1.59
Al	0.56	0.27
Si	0.55	0.26
Ca	0.51	0.17

Thermal gravimetric analysis (TGA) was used to determine the effect of structural differences on operating temperature and degradation behavior of biochar-S samples and watermelon peels. Each sample was cooked in an N_2 environment from ambient temperature to 1,000°C. TGA and differential thermal analysis (DTA) analytical curves for raw watermelon peels and biochar-S are shown in Fig. 4a. The first weight loss peaks occurred before 100°C, due to H_2O evaporation in the watermelon peel and biochar-S. As the temperature raised above 100°C, various acidic oxygen functional groups were broken down, causing raw watermelon peels and biochar-S to lose weight. Also, acidic groups such as phenol degrade at higher temperatures, while acidic groups such as lactones, anhydrides and carboxylic

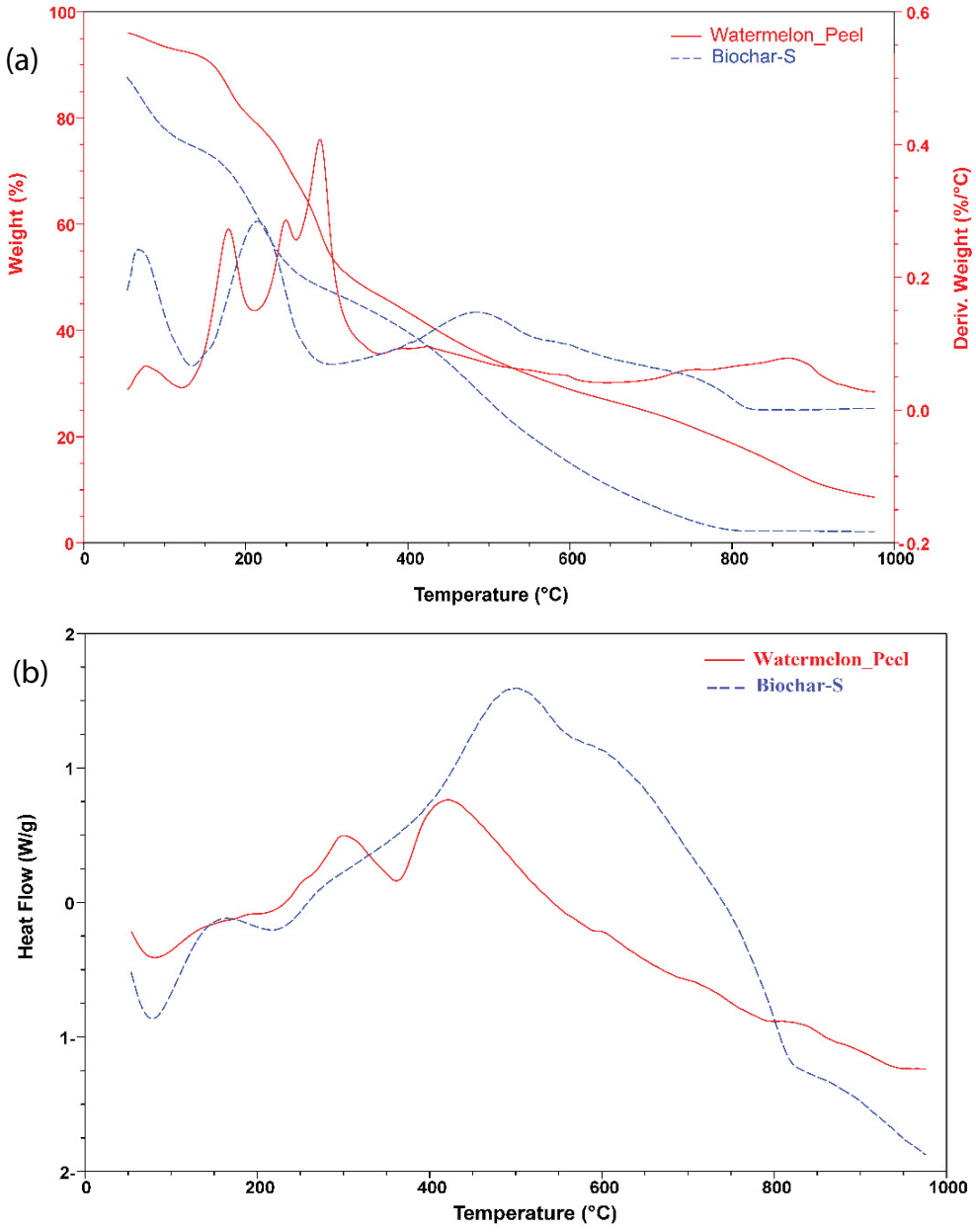

Fig. 4 Graphs of (a) TGA and DTA and (b) DSC analyses of the raw watermelon peels and biochar-S samples.

decompose at lower temperatures. Raw watermelon peels and biochar-S exhibit a minor plateau of weight loss at temperatures up to 450°C. Both TGA curves converged at temperatures greater than 450°C due to carbon breakdown in the material structure. At the final temperature of 1,000°C, various weight loss percentages of 39.56% and 45.12% were obtained with an order of watermelon peels biochar-S. The weight of the watermelon-peel biochar-S remained constant, and percentages of 12.62% and 14.50% were attained.

DTA graph of biochar-S and watermelon peels is illustrated in Fig. 4a. When Fig. 4a is examined, the DTA curves of the watermelon peels (red) peaked at six points at a low temperature (T_f, 76.93°C, 177.63°C, 250.50°C, 291.80°C, 425.89°C, and 871.64°C), while the curves of biochar-S (blue) peaked at only three points at the flow temperature (T_f, 75.11°C, 214.57°C, and 488.89°C). As can be seen from the DTA curves to produce biochar-S adsorbents from watermelon peels, dehydration of watermelon peels (red) showed three well-resolved degradation bands. The degradation bands of watermelon peel (red) decreased from six to three after treatment with H_2SO_4, indicating that the degree of degradation was strongly affected by acid treatment dehydration.

Thermal transitions can be used to compare materials using differential scanning calorimetry (DSC). The DSC profile of watermelon peels (red) and biochar-S is shown in Fig. 4b (blue). Watermelon peels exhibit crystallization temperatures T_C below 100°C, but biochar-S exhibits crystallization temperatures T_C between 225.10°C and 818.96°C. As the temperature is increases, watermelon peels melt at 297.62°C and 422.87°C, while biochar-S melts at 486.75°C. Watermelon peel exhibited a lower T_m, whereas biochar-S exhibited the greatest T_m. As a result of the higher transitional temperatures, the grains developed a greater degree of crystallinity, which increased their structural stability while also increasing their gelatin resistance.

3.2. Adsorption of Cu^{2+} ions on biochar-S

3.2.1. Effect of solution pH

The pH of the experimental solution is a parameter that significantly affects adsorption process. The amino, carboxyl, and hydroxyl groups on the biochar surface are highly affected by the solution pH. Determination of the quantity of Cu^{2+} ions adsorbed at equilibrium (q_e) and removal of these ions; achieved at 25°C, at a begining Cu^{2+} ions concentration of 50 mg L^{-1} and using 1.0 g L^{-1} biochar-S as adsorbent. In the pH values ranged between 2.33 and 6.1, the removal of Cu^{2+} ions was studied in 24 h of mexing time and the pH effect is illustrated in Fig. 5. For the removal of Cu^{2+} ions using biochar-S, it is seen in Fig. 5a that the highest Cu^{2+} ions removal (78%) occurred at pH 5.6. The relationship between the amounts of Cu^{2+} ions to biochar-S at equilibrium (q_e, mg g^{-1}) in the pH range varying from 2.33 to 6.1 is illustrated in Fig. 5b. The removal of Cu^{2+} ions to biochar-S showed that the pH value increased regularly from 2.33 to 6.1, the amounts of Cu^{2+} ions adsorbed at equilibrium (q_e) increased from 59 to 155 mg g^{-1}, respectively. It was determined that the optimum pH value for the removal of Cu^{2+} ions for biochar-S was 5.6.

In this study, the adsorption mechanism is as follows: the copper ions, which were originally 2+ charged, do not want to interact with the positively charged biochar-S. Negatively charged SO_4^{2-} groups are attached to the surface of biochar-S by interacting with H_2SO_4. Therefore, an attraction force occurs between Cu^{2+} ions and SO_4^{2-} functional groups, which has a positive effect on adsorption.

3.2.2. Mexing time effect

In the adsorption process, the mexing time is a significant parameter for the adsorbent to provide the necessary interaction with the adsorbate. Therefore, in this study, the

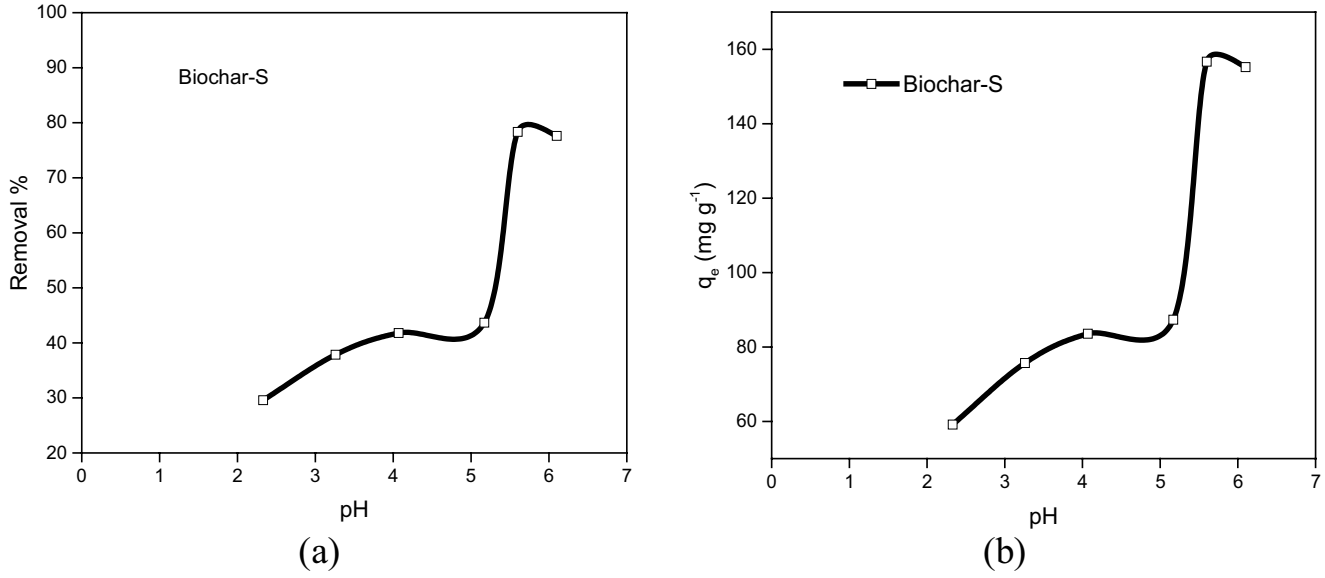

Fig. 5. (a) Cu^{2+} ions adsorption on biochar-S as a function of pH on the removal percentage and (b) on the q_e (mg g^{-1}) of Cu^{2+} ions (Cu^{2+} = 200 mg L^{-1}, biochar-S = 1.0 g L^{-1}, temperature = 25°C ± 2°C).

mexing time required for the removal of Cu^{2+} ions using biochar-S was also carried out. The effect of mexing time was investigated using biochar-S at pH 5.6, at Cu^{2+} ions initial concentration varying from 50 to 300 mg L^{-1}. Fig. 6a shows that 45%–75% of Cu^{2+} ions' removal takes place in the first 15–30 min. The removal of Cu^{2+} ions raised regularly with increasing mexing time, and at the end of 3 h, removal was between 54% and 82%, depending on the changing initial Cu^{2+} ions concentrations (300, 200, 150, 100, 75 and 50 mg L^{-1}). At the end of 24 h, it was observed that there was no significant change in Cu^{2+} ions beginning concentrations (300, 200, 150, 100, 75 and 50 mg L^{-1}), and the values were measured as 59%, 62%, 62%, 74%, 80% and 83%, respectively (Fig. 6b).

In Fig. 6, it can be deduced that Cu^{2+} ions removal occurs very rapidly in the first 15 min and Cu ion removal rises with decreasing biochar-S dosage. Maximum 82% removal was achieved by using biochar-S adsorbent.

3.2.3. Effect of Cu^{2+} ions begining concentration

The begining concentration of the adsorbed substance is also an significant parameter in adsorption studies. The effect of begining Cu^{2+} ion concentration on the adsorption capacity at equilibrium (q_e) was investigated. To determine the effect of biochar-S dosage on adsorption capacity at equilibrium (q_e), the adsorbent concentration (1, 2, 2.5, 3.0 and 4.0 g L^{-1}) and the initial Cu^{2+} ions concentration (50, 75, 100, 150, 200 and 300 mg L^{-1}) was studied at 25°C at a pH of 5.6. It can be seen from Fig. 7 that the adsorbed amount of Cu^{2+} ions at the same initial concentration of Cu^{2+} ions decrease at equilibrium (q_e) with the rise in biochar-S dosages. Fig. 7 shows the adsorption capacities at equilibrium (q_e) in removing Cu^{2+} ions using biochar-S adsorbent at different dosages (1.0–4.0 g L^{-1}). These values range from 34.60 to 130.42, 19.65 to 73.19, 16.2 to 62.16, 13.54 to 56.18 and 10.43 to 44.48 mg g^{-1} for initial Cu^{2+} ions concentrations (50, 75, 100, 150, 200 and 300 mg L^{-1}), respectively. The effect of the initial Cu^{2+} ions concentration on the adsorption capacity of Cu^{2+} ions on biochar-S was investigated, and the adsorption capacity at equilibrium (q_e) was higher in solutions with high initial Cu^{2+} ions concentration. It was observed that it decreased as the adsorbent dosage increased. The decline in the equilibrium (q_e) value of the concentration of Cu^{2+} ions solutions with increasing adsorbent mass and the concentration relationship between the adsorption vacancies of the biochar-S adsorbent explain the decrease in the equilibrium (q_e) value.

3.2.4. Effect of adsorbent dose

By using biochar-S adsorbent in different dosages (1.0–4.0 g L^{-1}), the begining concentration of Cu^{2+} ions (50–300 mg L^{-1}), adsorption time (3.5 h) and solution temperature (25°C) were studied at pH 5.6 and are illustrated in Fig. 8. Experimental data reveal that the removal percentage of Cu^{2+} ions (%) increases with the increase of biochar-S

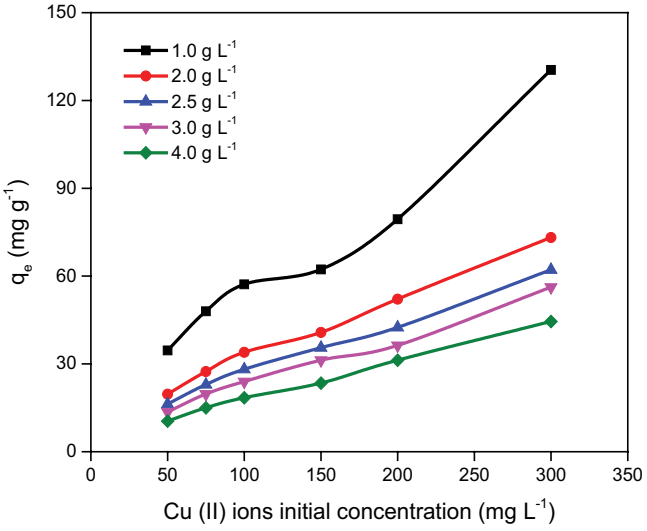

Fig. 7. Effect of Cu^{2+} ions initial concentration (50–300 mg L^{-1}) using biochar-S dosages (1.0–4.0 g L^{-1}) on q_e (mg g^{-1}) (temperature = 25°C ± 2°C).

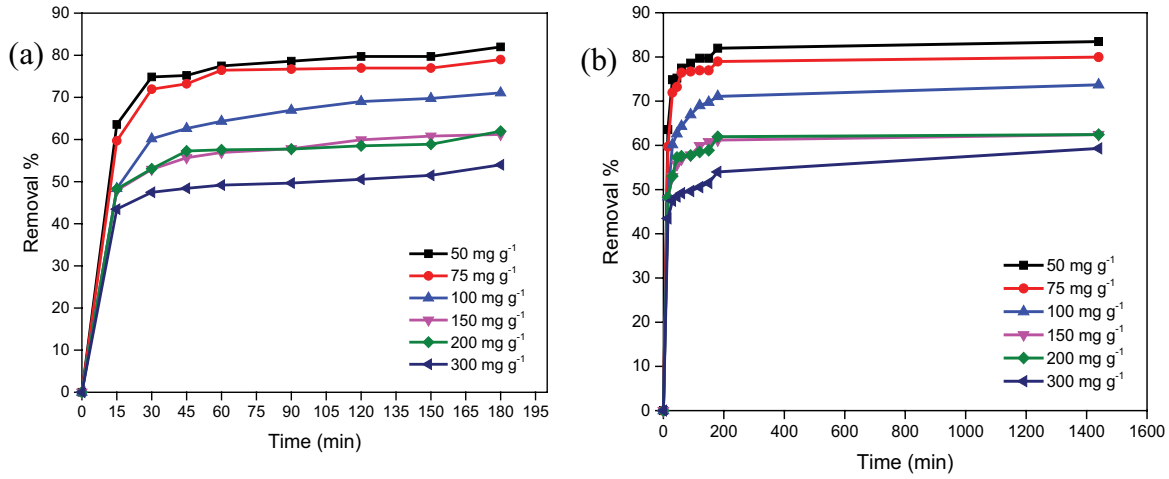

Fig. 6. Removal of Cu^{2+} ions (a) the first 3 h and (b) the first 24 h using biochar-S as an adsorbent (beginning concentration of Cu^{2+} ions: (50–300 mg L^{-1}), biochar-S dosage = 4.0 g L^{-1}, temperature = 25°C ± 2°C.

dosage, while the amount of Cu^{2+} ions (q_e) adsorbed at equilibrium decreases.

When the amount of biochar-S adsorbent increases from 1.0 to 4.0 g L^{-1}, for the begining Cu^{2+} ions concentrations (50, 75, 100, 150, 200, and 300 mg L^{-1}) the percentage of removal of Cu^{2+} ions enhance from 69% to 83%, 64% to 80%, 57% to 74%, 42% to 62%, 40% to 62%, and 43% to 59%, respectively. Furthermore, the amount of Cu^{2+} ions adsorbed at equilibrium (q_e) decreases from 34.60 to 10.43, 47.96 to 15.00, 57.18 to 18.43, 62.27 to 23.42, 79.43 to 31.22, and 130.42 to 44.48 mg g^{-1} with increasing of the amount of biochar-S from 1.0 to 4.0 g L^{-1} for beginning Cu^{2+} ions concentrations 50, 75, 100, 150, 200 and 300 mg L^{-1}, respectively. It was determined that the minimum adsorption amount at equilibrium (q_e) and the maximum removal percentage of Cu^{2+} ions were obtained by using 4.0 g L^{-1} biochar-S adsorbent dosage.

3.3. Adsorption isotherms

The correlation between the adsorbate concentration at the equilibrium time (C in mg L^{-1}) and the mass of the adsorbent (q_e mg g^{-1}) is explained by the adsorption isotherm, and this isotherm explains the state of adsorbate molecules dispersed between solid-liquid phases [68,90]. Isotherm data should be examined to define the adsorbate molecular fraction distributed at equilibrium (q_e) between the solid and liquid phases and to optimize the use of adsorbent. There are several isotherm models which help for the mentioned calculations; the data obtained were analyzed with Langmuir, Freundlich, Temkin and Dubinin–Radushkevich isotherm models [68] to rationalize the Cu^{2+} ions and melon-biochar interactions observed in this study.

The equilibrium adsorption constant related to the saturated monolayer adsorption capacity (Q_m) and the affinity of the adsorption sites (K_L) are the Langmuir constants and the values obtained for the adsorption of Cu^{2+} ions onto biochar-S adsorbent are illustrated in Table 3. The linear form of the Langmuir model showed a high correlation coefficient ($R^2 \geq 0.901$) when the biochar-S dosage was 2.5 g L^{-1}, and the maximum monolayer capacity (Q_m) of the biochar-S adsorbent was calculated as 151.52 mg g^{-1}. The $1/Q_mK_L$ and $1/Q_m$ values of the Langmuir model are acquired from the intersection point and slope of the line graph, respectively, by plotting C_e/q_e vs. C_e as seen in Fig. 9a. It was calculated from the Langmuir isotherm model that the maximum monolayer capacity (Q_m) of biochar-S, obtained in the adsorption of Cu^{2+} ions, was 151.52 mg g^{-1} (Table 3). The equilibrium adsorption constant (K_L) ranging from 0.01 to 0.02 L mg^{-1} and the correlation coefficient ($R^2 \geq 0.901$) obtained for the linear form of the Langmuir model are strong positive proof for the adsorption of Cu^{2+} ions on biochar-S. It is understood that the applicability of Cu^{2+} ions to adsorb on biochar-S is possible according to the Langmuir isotherm model. It is possible to conclude that Cu^{2+} ions are adsorbed in a monolayer on the biochar-S adsorbent surface. Another model used by biochar-S for the removal of Cu^{2+} ions is the Freundlich model. Freundlich isotherm model was used to determine the efficiency of biochar-S adsorbent in removing Cu^{2+} ions. Although this model correctly establishes the adsorption process as a heterogeneous phenomenon, Table 3 shows the linear fitting parameters obtained from the model. In the plot of $\log(q_e)$ vs. $\log(C_e)$ (Fig. 9b), the intercept value and the slope of the graph give $\log K_F$ and $1/n_F$, respectively. One of the Freundlich constants, K_F (L g^{-1}) represents the binding energy. K_F, which represents the amount of Cu^{2+} ions adsorbed on the adsorbent for unit equilibrium concentration, can be expressed as the distribution or adsorption coefficient. Generally, the rice in the adsorption capacity of the adsorbent is directly proportional to the rise in the K_F value. In the Freundlich model, the easy adsorbing of the solute by the adsorbent depends on the $1/n$ value being less than 1. In such cases, the removal of Cu^{2+} ions on the adsorbent is a suitable physical process. It can be attributed to the fact that the $1/n$ values are less than one, which is suitable for the removal of Cu^{2+} ions using biochar-S adsorbent. Also, the degree of nonlinearity between the adsorption process and the solution

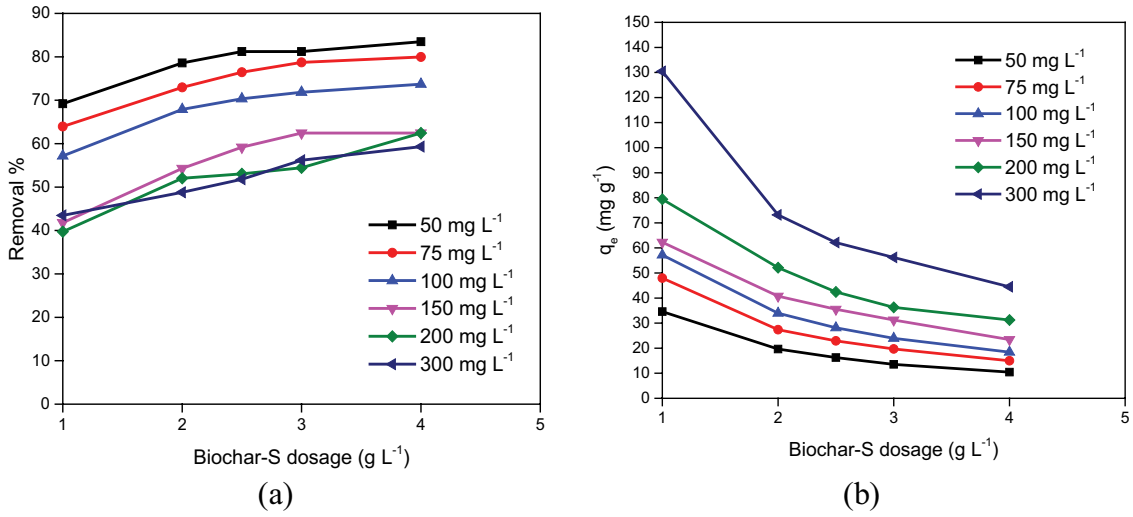

Fig. 8. Effect of biochar-S different dosages (1.0–4.0 g L^{-1}) of different beginning Cu^{2+} ions concentration (50–300 mg L^{-1}) (a) on removal percentage and (b) on q_e (mg g^{-1}), (temperature = 25°C ± 2°C).

Table 3
Isotherm study data of adsorption of Cu^{2+} ions onto biochar-S adsorbent (Initial Cu^{2+} ions concentration = (50–300 mg L^{-1}), adsorbent dosages = (1.0–4.0 g L^{-1}), temperature = (25°C ± 2°C)

Isotherm model	Parameters	Biochar-S adsorbent dosages (g L^{-1})				
		1.0	2.0	2.5	3.0	4.0
Langmuir	Q_m (mg g^{-1})	151.52	89.29	73.53	66.23	56.50
	K_L	0.01	0.02	0.02	0.02	0.02
	R^2	0.727	0.897	0.901	0.864	0.858
Freundlich	$1/n$	0.46	0.46	0.45	0.48	0.50
	Q_m (mg g^{-1})	70.0	47.0	41.0	43	36
	K_F ($mg^{1-1/n}$ $L^{1/n}$ g^{-1})	9.76	6.67	6.02	4.84	3.63
	R^2	0.890	0.974	0.977	0.963	0.972
Temkin	A_T	0.13	0.13	0.15	0.15	0.14
	B_T	35.13	22.34	17.89	16.62	14.65
	R^2	0.835	0.955	0.941	0.923	0.963
Dubinin–Radushkevich	Q_m (mol kg^{-1})	79.47	47.88	40.21	35.84	27.90
	$K \times 10^6$ $(mol\ kJ)^{-2}$	38.10	20.30	16.10	17.20	13.70
	E (kJ mol^{-1})	114.56	156.94	176.23	170.50	191.04
	R^2	0.621	0.680	0.688	0.717	0.677

concentration is expressed by the n_F value. The fact that the removal of Cu^{2+} ions on biochar-S adsorbent is a suitable physical process depends on the value of n_F greater than 1.

The Freundlich isotherm correlation coefficient values obtained from Fig. 11b successfully describe the variation of $\log q_e$ as a function of $\log C_e$. Table 3 illustrated Freundlich Q_m is equal to 70 mg g^{-1} for the biochar-S adsorbent. Better removal of Cu^{2+} ions is possible with higher Q_m values. The correlation coefficient ($R^2 > 0.977$) was found for biochar-S adsorbent according to the Freundlich model. The Q_m value was 70 mg g^{-1} for biochar-S adsorbent. The highest Q_m value belongs to the adsorbent with a 1.0 g L^{-1} concentration (Table 3).

The third model applied to the experimental data was the Temkin model. The Temkin model is used to explain the effects of indirect adsorbate/adsorbent interactions on the adsorption process. The heat exchange occurring during adsorption is taken into account by this model and it is assumed that the adsorption heats of all molecules in the layer decrease linearly as a result of the surface being covered with adsorbate molecules. Temkin isotherm parameters of the adsorption of Cu^{2+} ions by biochar-S were obtained from Fig. 9c. As seen in Fig. 9c, The Temkin constants (A_T and B_T) are calculated using the linear relationship between q_e and $\ln C_e$. While A_T, which is the equilibrium binding constant (L g^{-1}), is calculated from the slope in the graph, B_T, which expresses the adsorption heat coefficient, is calculated from the intercept. The Temkin constants were estimated and listed in Table 3. The Temkin isotherm correlation coefficient value ($R^2 > 0.963$) obtained in the removal of Cu^{2+} ions on the biochar-S surface with a dosage of 4.0 g L^{-1} shows that this model is suitable for examining the temperature changes in the adsorption process. The presence of very weak ionic interaction between the adsorbent and the adsorbate and the fact that the removal process of Cu^{2+} ions includes physisorption can be attributed to the very low heat of sorption. The coating of Cu^{2+} ions on biochar-S adsorbent occurs as a result of adsorbent–adsorbate interaction and this interaction is related to the heat of adsorption B_T. It is shown in Table 3 that this value decreased with the rise of biochar-S adsorbent dosages. To investigate the mode of adsorption of Cu^{2+} ions onto biochar-S adsorbent (whether it is chemical or physical in natura), the equilibrium data was also applied to the Dubinin–Radushkevich isotherm model. The Dubinin–Radushkevich isotherm model is based on the Polanyi potential theory, which is applied where the adsorption process continues until the pores are filled. Table 3 illustrates the Dubinin–Radushkevich isotherm constants and the correlation coefficients obtained for the removal of Cu^{2+} ions. The apparent energy E value is used to predict the type of adsorption. If the E value is less than 8 kJ mol^{-1}, in the range of 8–16 kJ mol^{-1}, or greater than 16 kJ mol^{-1}, the adsorption type is considered as physical adsorption, ion exchange, and chemical adsorption, respectively [91,92]. The estimated values of bonding energy (E) for the present study were found to be >16 kJ mol^{-1} for all adsorbent dosage, which implies that adsorption of Cu^{2+} ions onto biochar-S adsorbent is by chemical adsorption. In the Dubinin–Radushkevich model, the R^2 values ranged from 0.621 to 0.717 for Cu^{2+} ions by the biochar-S adsorbent (Fig. 9d; Table 3).

3.4. Statistical error function analysis of isothermal models

Experimental equilibrium data of Cu^{2+} ions on biochar-S were analyzed with the most used isotherm models (Langmuir, Freundlich, Temkin and Dubinin–Radushkevich). By using several different error functions, the most suitable isotherm model was determined for the experimental data. To determine the error distribution between experimental equilibrium values and predicted isotherm models, average percentage errors (APE), hybrid error function (HYBRID), Chi-square error (χ^2), the sum of the absolute errors (EABS),

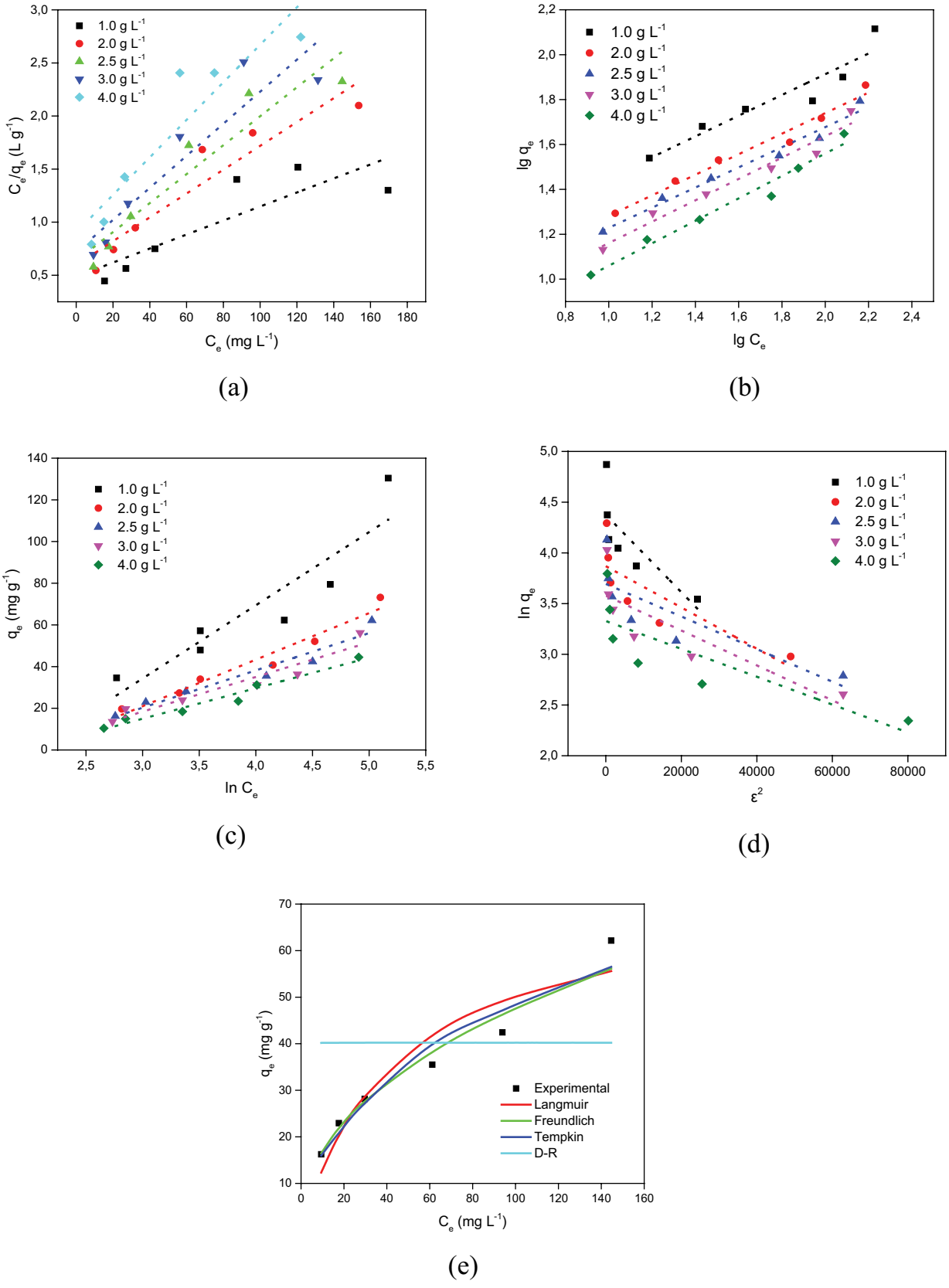

Fig. 9. (a) Linearized Langmuir, (b) Freundlich, (c) Temkin, (d) Dubinin–Radushkevich, and (e) comparison of measured and modeled isotherm profiles for Cu^{2+} ions of initial concentration (50–300 mg L^{-1}) on biochar-S dosages (1.0–4.0 g L^{-1}) at (25°C ± 2°C).

the root mean square errors (RMS) and MPSD are used [68]. Table 4 shows the six error functions expressing the similarity between the experimental data of the watermelon-biochar-S adsorbent and the values calculated using the theoretical isotherms. If Table 4 is examined, it will be seen that the error functions values of RMS, χ^2, APE, EABS, MPSD and HYBRID in the Freundlich model, which is the most suitable isotherm model for melon-biochar, are lower than those in other models.

3.5. Adsorption kinetics

For the kinetic models of adsorption of Cu^{2+} ions on biochar-S adsorbent, pseudo-first-order, pseudo-second-order, Elovich and intraparticle diffusion equations are applied [68]. Correlation coefficients (R^2), which take a value between zero (0) and one (1), determine the suitability of the models, and the closer this value is to one, the model is interpreted as a suitable model. The equilibrium adsorption capacity (q_e) and the rate constant, k_1 were determined using straight-line plots of $\log(q_e - q_t)$ vs. t (Fig. 10a). Correlation coefficients (R^2) of – biochar-S for different Cu^{2+} ions initial concentrations and adsorbent dosages are shown in Tables 5 and 6.

The low R^2 values obtained from the graphs of the pseudo-first-order rate equations indicate that the evaluated q_e values deviate greatly from the experimental values. This shows that the pseudo-first-order reaction equation is not very suitable for the adsorption of Cu^{2+} ions on the

Table 4
A few error function values of the isotherm models best suited to the experimental equilibrium data in the adsorption of Cu^{2+} ions on biochar-S

Isotherm model	APE (%)	χ^2	HYBRID	MPSD	EABS	RMS
Langmuir	14.84	33.31	15.90	17.41	177.38	16.82
Freundlich	7.07	15.62	7.58	9.58	111.39	9.26
Temkin	10.30	19.65	11.04	12.48	134.56	12.06
Dubinin–Radushkevich	55.33	362.12	59.28	76.20	488.13	73.62

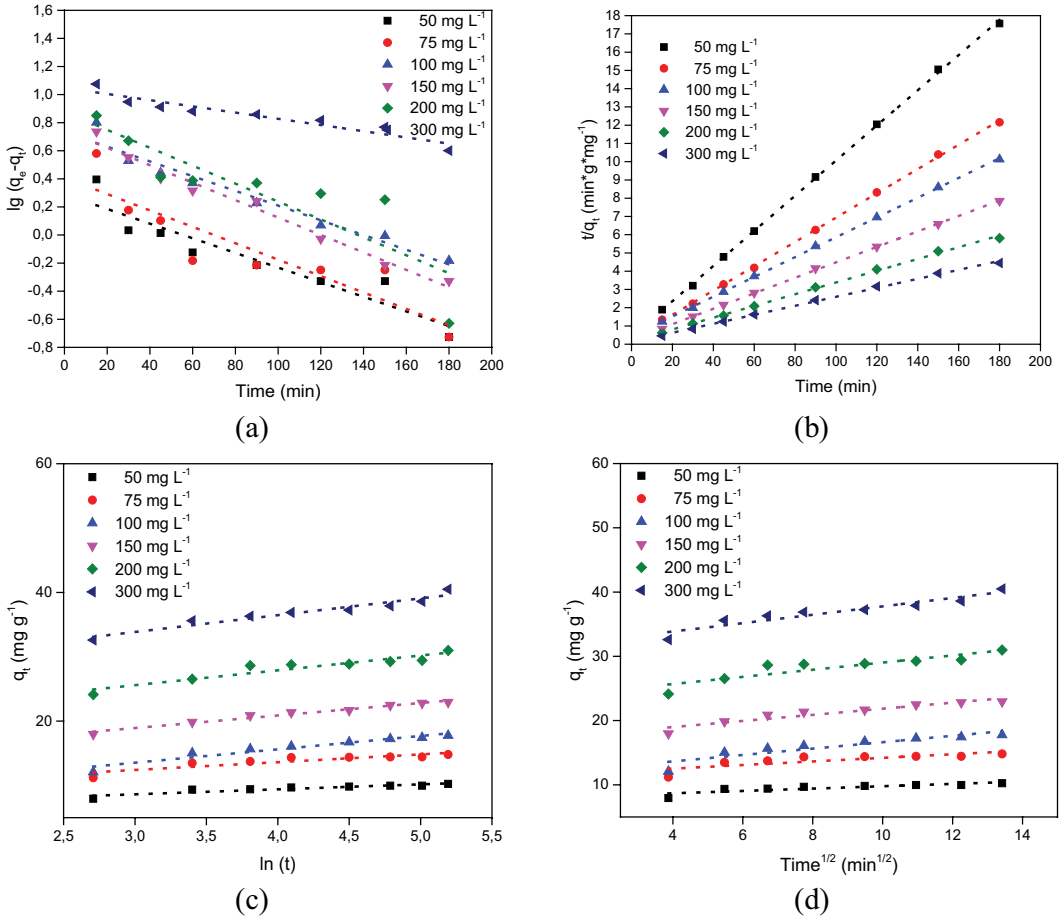

Fig. 10. (a) Pseudo-first-order, (b) pseudo-second-order, (c) Elovich, and (d) intraparticle diffusion model of adsorption of Cu^{2+} ions by biochar-S adsorbent (initial concentration = (50–300 mg L^{-1}), adsorbent dosage = (4.0 g L^{-1}), temperature = 25°C ± 2°C).

Table 5
Pseudo-first-order and pseudo-second-order kinetic model results of adsorption of Cu^{2+} ions by biochar-S adsorbent (Cu^{2+} ions beginning concentration = (50–300 mg L^{-1}), biochar-S dosages = (1.0–4.0 g L^{-1}), temperature = (25°C ± 2°C)

Parameter			Pseudo-first-order			Pseudo-second-order			
Biochar-S dosages (g L^{-1})	Cu(II) ion (mg L^{-1})	q_e (exp.)	q_e (calc.)	$k_1 \times 10^3$	R^2	q_e (calc.)	$k_2 \times 10^3$	h	R^2
1.0	50	34.60	15.01	18.42	0.892	36.23	2.22	2,913	0.995
	75	47.96	12.05	13.36	0.836	49.02	2.59	6,231	0.998
	100	57.18	13.61	8.06	0.844	54.95	3.21	9,699	1.000
	150	62.27	16.38	17.04	0.892	64.94	1.99	8,375	0.999
	200	79.43	22.36	16.58	0.726	79.37	2.19	13,774	0.998
	300	130.42	26.23	4.61	0.946	120.48	2.03	29,412	0.999
2.0	50	19.65	5.37	7.60	0.812	18.66	8.07	2,807	1.000
	75	27.36	4.05	9.90	0.784	27.03	10.32	7,541	1.000
	100	33.94	10.30	16.12	0.987	34.60	3.74	4,474	1.000
	150	40.73	12.63	15.89	0.900	41.84	3.81	6,662	1.000
	200	52.11	16.22	11.05	0.905	51.55	2.25	5,977	0.998
	300	73.19	29.57	12.44	0.909	73.53	1.07	5,811	0.992
2.5	50	16.24	4.19	7.14	0.802	15.36	10.67	2,518	0.999
	75	22.94	4.80	16.58	0.935	23.26	8.73	4,724	1.000
	100	28.13	6.93	8.98	0.860	27.40	5.76	4,323	0.999
	150	35.51	9.20	15.20	0.863	36.63	3.47	4,658	0.998
	200	42.44	8.56	9.44	0.943	41.67	4.79	8,313	1.000
	300	62.16	15.81	10.59	0.891	61.35	2.44	9,166	1.000
3.0	50	13.54	2.25	10.13	0.871	13.37	18.46	3,299	1.000
	75	19.68	3.52	12.44	0.815	19.69	11.26	4,363	1.000
	100	23.94	6.67	10.36	0.922	23.53	5.73	3,170	0.999
	150	31.22	7.30	11.05	0.978	30.96	5.35	5,126	1.000
	200	36.31	7.97	14.97	0.904	36.50	5.41	7,210	0.999
	300	56.18	13.26	4.84	0.690	51.02	4.56	11,876	1.000
4.0	50	10.43	1.95	11.98	0.881	10.38	21.43	2,311	1.000
	75	14.99	2.56	13.36	0.811	15.02	16.14	3,639	1.000
	100	18.43	5.42	11.98	0.951	18.45	6.73	2,290	1.000
	150	23.42	5.56	14.28	0.979	23.64	7.14	3,990	1.000
	200	31.22	7.52	14.74	0.756	31.06	6.15	5,935	0.998
	300	44.48	11.18	5.07	0.898	40.65	4.40	7,273	0.998

biochar-S adsorbent (Tables 5 and 6). When the correlation of the experimental data of biochar-S adsorbent with the pseudo-first-order model was examined, it was determined that there was no regular rise or decrease in R^2 values with the rise of the beginning adsorbent concentration from 1.0 to 4.0 g L^{-1}.

The kinetics of Cu^{2+} ions adsorption over biochar-S adsorbents following the pseudo-second-order was studied. The quantity of Cu^{2+} ions adsorbed at equilibrium (q_e) and the pseudo-second-order kinetic constant, k_2 (g mg^{-1} min^{-1}) are calculated by plotting t/q_e vs. t as shown in Fig. 10b. Fig. 10b shows pseudo-second-order kinetic plots for the removal of Cu^{2+} ions over biochar-S adsorbents. Table 5 shows the experimentally and theoretically predicted q_e values, the kinetic constant k_2, and their corresponding R^2 values. When Table 5 is examined, it is seen that the pseudo-second-order model is the model with R^2 values closest to 1. Therefore, the most suitable kinetic model is the pseudo-second-order model. In addition, for all initial Cu^{2+} ions concentrations studied, the q_e values evaluated using the pseudo-second-order kinetic model graph also overlap exactly with the experimental q_e values.

The correlation curve between q_t and ln(t) is shown in Fig. 10c. Elovich constant α was calculated from the intercept of this figure and Elovich constant β was calculated from its slope and shown in Table 6. If the R^2 values are compared, it can be said that the R^2 values of the Elovich model have similar values with the pseudo-first-order kinetic model. At some initial concentrations, the Elovich model fits the experimental data better, while at different initial concentrations, the pseudo-first-order kinetic model seems to fit better. Both models did not fit as well as the pseudo-second-order kinetic model (Tables 5 and 6). The results indicate that the chemical adsorption during the removal of Cu^{2+} ions on the biochar-S adsorbent can be rate-limiting in some cases. However, the fact that the R^2 values are

Table 6
Elovich and intraparticle diffusion models results from the adsorption of Cu^{2+} ions by biochar-S adsorbent (Cu^{2+} ions begining concentration = (50–300 mg L^{-1}), biochar-S dosages = (1.0–4.0 g L^{-1}), temperature = (25°C ± 2°C)

Parameter		Elovich			Intraparticle diffusion		
Biochar-S dosages (g L^{-1})	Cu(II) ion (mg L^{-1})	β	α	R^2	K_{dif}	C	R^2
1.0	50	0.22	44.32	0.837	1.16	19.54	0.826
	75	0.16	100.90	0.812	1.42	30.28	0.678
	100	0.20	1,558.26	0.935	1.20	39.05	0.835
	150	0.13	230.03	0.887	1.78	41.05	0.789
	200	0.19	52,507.05	0.923	1.35	60.11	0.897
	300	0.18	33,896,817.66	0.931	1.44	99.53	0.937
2.0	50	0.50	116.60	0.902	0.47	12.37	0.781
	75	0.51	12,374.64	0.742	0.45	21.29	0.606
	100	0.28	243.04	0.977	0.88	22.58	0.900
	150	0.25	626.77	0.930	0.97	28.85	0.826
	200	0.18	273.88	0.918	1.33	32.80	0.839
	300	0.14	521.53	0.859	1.91	44.06	0.946
2.5	50	0.68	238.98	0.899	0.35	10.65	0.789
	75	0.49	1,005.74	0.870	0.48	16.99	0.739
	100	0.39	585.54	0.873	0.61	19.15	0.768
	150	0.32	1,556.95	0.958	0.78	25.32	0.955
	200	0.35	30,231.15	0.965	0.70	31.97	0.906
	300	0.16	623.22	0.938	1.49	41.43	0.842
3.0	50	1.05	6,476.78	0.861	0.22	10.42	0.739
	75	0.57	775.27	0.845	0.41	14.46	0.703
	100	0.42	210.23	0.919	0.57	15.66	0.825
	150	0.40	2,962.37	0.981	0.61	22.54	0.923
	200	0.38	12,019.94	0.925	0.64	27.73	0.839
	300	0.24	5,172.80	0.800	0.96	38.51	0.665
4.0	50	1.29	2,718.96	0.858	0.18	7.95	0.743
	75	0.83	1,740.25	0.800	0.28	11.41	0.661
	100	0.48	70.18	0.932	0.50	11.65	0.831
	150	0.51	1,618.82	0.975	0.48	17.09	0.901
	200	0.43	7,587.00	0.887	0.56	23.47	0.800
	300	0.38	5.07	0.930	0.65	31.25	0.901

not very high makes it possible to have physical adsorption in the process.

Intraparticle diffusion is a model used to explain the transfer of solute in solid–liquid adsorption. In this study, as it is necessary to identify and explain the stages involved in the sorption process the intraparticle diffusion model was used. Adsorption of an adsorbate to an adsorbent takes place in 3 steps: (i) In the first step, the ions/molecules adsorbed by the adsorbent move from the solution through the liquid film to the surface of the adsorbent particles. (ii) The molecules attached to the surface slowly diffuse into the adsorbent after this stage. (iii) A chemical reaction takes place very quickly in the active groups of the adsorbent particles. The speed of all three steps can be effective in determining the rate of adsorption, and the step with the slowest speed also determines the rate of adsorption.

When the square root values of q_t and time (t) are plotted, if a line passes through the origin, it was determined by Weber and Morris [65] that the adsorption is controlled by the intraparticle diffusion step. On the other hand, if the line does not pass through the origin (where the C value is large), it is understood that the film diffusion largely determines the rate of the adsorption process. The Webber-Morris adsorption line of the removal of Cu^{2+} ions on biochar-S adsorbent at different adsorbent dosages and different initial Cu^{2+} ion concentrations is illustrated in Fig. 10d. The C and K_{dif} values shown in Table 6 were evaluated from the intercept point and slope of the plot of q_t vs. $t^{0.5}$, respectively. It can be seen from Fig. 10d that the C intercept is quite large and the straight lines do not pass through the origin. This indicates that the rate of adsorption gradually rises over time and that this rate is controlled by film diffusion, not intraparticle diffusion. This can be explained by the decrease in biochar-S surface area and pore volume overtime during the adsorption process. In addition, it was determined that the C value increased continuously both with the increase

of biochar-S dosage and with the increase of the initial Cu^{2+} ions concentration.

3.6. Comparison with results reported in the literature

In the literature review summarized in Table 7, the effectiveness of the removal of Cu^{2+} ions using different adsorbents was compared with the biochar-S adsorbent and showed that biochar-S adsorbent was effective in removing Cu^{2+} ions.

3.7. Regeneration of biochars

3.7.1. Desorption and regeneration studies

Desorption experiments of Cu^{2+} ions from the loaded biochar-S were performed using 0.1 N HCl and 0.1 M NaOH as eluted mediums to investigate the economic feasibility and reusability of biochar-S adsorbent. In this condition the desorption % decreased with rising regeneration cycles Fig. 11a. The regenerated biochar-S was applied in six consecutive cycles of adsorption/desorption. The adsorption amount presented was consistent through the cycles and experienced the adsorption capacity decreased by 3.27% after six generations which suggests it may be used as a sustainable Cu^{2+} ions dye removal (Fig. 11b).

4. Conclusion

In this work, we have demonstrated that watermelon peels, an agricultural waste, can be used as cheap and effective materials for the production of biochar-S. The obtained biochar-S was prepared by treatment of dry watermelon peels with 50% H_2SO_4 at boiling point and the efficiency of biochar-S in the removal of Cu^{2+} ions was tested. The sorption of Cu^{2+} ions was found to be dependent on initial concentration, adsorbent dosage, pH and the contact time between the adsorbent and adsorbate. It was determined that the optimum pH value for the adsorption of Cu^{2+} ions by biochar-S was 5.6. It was determined that the minimum adsorption amount at equilibrium (q_e) and the maximum removal percentage of Cu^{2+} ions were obtained by using 4.0 g L^{-1} biochar-S adsorbent dosage. In the removal of Cu^{2+} ions, the Freundlich model is a better sorption

Table 7
Comparison of the maximum adsorption capacities of Cu^{2+} ions of different adsorbents

Adsorbents	Max. capacity (mg g^{-1})	Max. removal (%)	Reference
Sawdust	1.79	98.8	[91]
Saccharomyces cerevisiae	1.90	90.0	[94]
Orange peel	3.65	–	[95]
Tea fungal biomass	4.64	58.0	[96]
Datura innoxia	7.20	92.0	[97]
Tree fern	11.7	–	[98]
Banana peel	8.24	81.2	[99]
Sugarcane bagasse	9.48	91.2	[99]
Watermelon rind	5.73	56.4	[99]
Natural zeolite	141.12	66.10	[16]
Biochar-S	151.52	78.33	This work

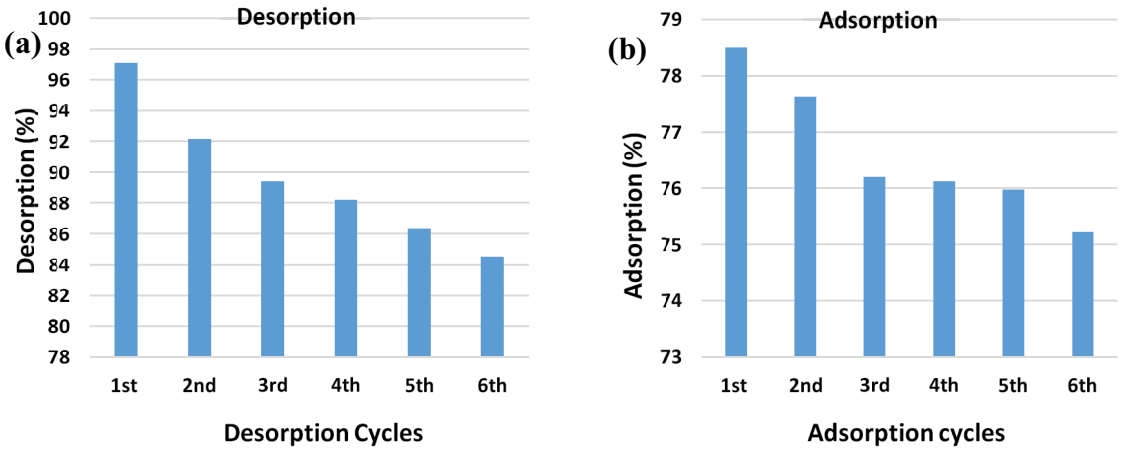

Fig. 11. (a) Desorption percentage of Cu^{2+} ions from biochar-S using 0.1 N HCl and 0.1 M NaOH. (b) Adsorption cycles of Cu^{2+} ions by regenerated biochar-S by 0.1 N HCl and 0.1 M NaOH.

process than other models. Although the sorption of Cu^{2+} ions onto biochar-S adsorbent was better described by the Freundlich model, the maximum adsorption capacity calculated by using the Langmuir isotherm as 151.52 mg g^{-1}. Adsorption energy obtained from Dubinin–Radushkevich isotherm models shows the chemisorption nature of the adsorption process. In conclusion. we believe that biochar-S obtained from watermelon peels may be successfully used to purify wastewaters containing toxic Cu^{2+} ions.

Acknowledgement

The corresponding author is grateful to the Science, Technology & Innovation Funding Authority (STDF) of Egypt for its partial financial support of this work (Project No. CB-4874 and CB-22816).

References

[1] A. El Nemr, G.F. El-Said, S. Ragab, A. Khaled, A. El-Sikaily, The distribution, contamination and risk assessment of heavy metals in sediment and shellfish from the Red Sea coast, Egypt, Chemosphere, 165 (2016) 369–380.
[2] A.M. Idris, T.O. Said, E.I. Brima, T. Sahlabji, M.M. Alghamdi, A.A. El-Zahhar, M. Arshad, A. El Nemr, Assessment of contents of selected heavy metals in street dust from Khamees-Mushait city, Saudi Arabia, using multivariate statistical analysis, GIS mapping, geochemical indices and health risk, Fresenius Environ. Bull., 28 (2019) 6059–6069.
[3] V.S. Aquib Jawed, L.M. Pandey, Engineered nanomaterials and their surface functionalization for the removal of heavy metals: a review, J. Water Process Eng., 33 (2020) 1–20.
[4] A. Alvarez, J.M. Saez, J.S.D. Costa, V.L. Colin, M.S. Fuentes, S.A. Cuozzo, C.S. Benimeli, M.A. Polti, M.J. Amoroso, Actinobacteria: current research and perspectives for bioremediation of pesticides and heavy metals, Chemosphere, 166 (2017) 41–62.
[5] A. El Nemr, Impact, Monitoring and Management of Environmental Pollution, Nova Science Publishers, Inc., Hauppauge, New York, 2011, 638 pages [ISBN-10: 1608764877, ISBN-13: 9781608764877].
[6] A. El Nemr, Environmental Pollution and its Relation to Climate Change, Nova Science Publishers, Inc., Hauppauge, New York, 2012, 694 pages [ISBN-13: 978-1-61761-794-2].
[7] A. El Nemr, Heavy Metals, Algae and Microbial Activities in Marine System, Nova Science Publishers, Inc., Hauppauge, New York, 2015, 663 pages [Hard Cover ISBN: 978-1-63482-314-2, e-Book. ISBN: 978-1-63482-315-9]
[8] M. Kumar, M. Nandi, K. Pakshirajan, Recent advances in heavy metal recovery from wastewater by biogenic sulfide precipitation, J. Environ. Manage., 278 (2021) 111555, doi: 10.1016/j.jenvman.2020.111555.
[9] A. El Nemr, Pollution Status, Environmental Protection, and Renewable Energy Production in Marine Systems, Nova Science Publishers, Inc., Hauppauge, New York, 2016 [Hard Cover ISBN: 978-1-63484-047-7, e-Book. ISBN: 978-1-63484-282-2].
[10] E. Malkoc, Ni(II) removal from aqueous solutions using cone biomass of *Thuja orientalis*, J. Hazard. Mater. B, 137 (2006) 899–908.
[11] A. El Nemr, A. El Sikaily, A. Khaled, O. Abdelwahab, Removal of toxic chromium(VI) from aqueous solution by activated carbon using *Casuarina equisetifolia*, Chem. Ecol., 23 (2007) 119–129.
[12] O. Abdelwahab, A. El Sikaily, A. Khaled, A. El Nemr, Mass transfer processes of chromium(VI) adsorption onto guava seeds, Chem. Ecol., 23 (2007) 73–85.
[13] H. Li, Z. Li, T. Liu, X. Xiao, Z. Peng, L. Deng, A novel technology for biosorption and recovery hexavalent chromium in wastewater by bio-functional magnetic beads, Bioresour. Technol., 99 (2008) 6271–6279.
[14] M.O.R. Uauy, M. Gonzalez, Essentiality of copper in humans, Am. J. Clin. Nutr., 67 (1998) 952–959.
[15] A.K. Sengupta, D. Clifford, S. Subramonian, Chromate ion-exchange process at alkaline pH, Water Res., 20 (1986) 1177–1184.
[16] E. Erdem, N. Karapinar, R. Donat, The removal of heavy metal cations by natural zeolites, J. Colloid Interface Sci., 280 (2004) 309–314.
[17] G. McKay, M.S. Otterburn, A.G. Sweeney, The removal of colour from effluent using various adsorbents—IV. Silica: equilibria and column studies, Water Res., 14 (1980) 21–27.
[18] A. Bhatnagar, A.K. Jain, A comparative adsorption study with different industrial wastes as adsorbents for the removal of cationic dyes from water, J. Colloid Interface Sci., 281 (2005) 49–55.
[19] U. Farooq, J.A. Kozinski, M.A. Khan, M. Athar, Biosorption of heavy metal ions using wheat based biosorbents – a review of the recent literature, Bioresour. Technol., 101 (2010) 5043–5053.
[20] M.A. Hassaan, A. El Nemr, F.F. Madkour, Testing the advanced oxidation processes on the degradation of Direct Blue 86 dye in wastewater, Egypt. J. Aquat. Res., 43 (2017) 11–19.
[21] M.A. Hassaan, A. El Nemr, F.F. Madkour, Advanced oxidation processes of Mordant Violet 40 dye in freshwater and seawater, Egypt. J. Aquat. Res., 43 (2017) 1–9.
[22] A. El Nemr, M.A. Hassaan, F.F. Madkour, Advanced oxidation process (AOP) for detoxification of Acid red 17 dye solution and degradation, Environ. Process., 5 (2018) 95–113.
[23] M.A. El-Nemr, I.M.A. Ismail, N.M. Abdelmonem, S. Ragab, A. El Nemr, Ozone and ammonium hydroxide modification of biochar prepared from *Pisum sativum* peels improves the adsorption of copper(II) from an aqueous medium, Environ. Process., 7 (2020) 973–1007.
[24] B.C.T. Robinson, P. Nigam, Removal of dyes from a synthetic textile dye effluent by biosorption on apple pomace and wheat straw, Water Res., 36 (2002) 2824–2830.
[25] J. Qi, Z. Li, Y. Guo, H. Xu, Adsorption of phenolic compounds on micro- and mesoporous rice husk-based active carbons, Mater. Chem. Phys., 87 (2004) 96–101.
[26] G. Yin, Z. Liu, Q. Liu, W. Wu, The role of different properties of activated carbon in CO_2 adsorption, Chem. Eng. J., 230 (2013) 133–140.
[27] M.A. El-Nemr, N.M. Abdelmonem, I.M.A. Ismail, S. Ragab, A. El Nemr, The efficient removal of the hazardous Azo Dye Acid Orange 7 from water using modified biochar from pea peels, Desal. Water Treat., 203 (2020b) 327–355.
[28] M.A. El-Nemr, N.M. Abdelmonem, I.M.A. Ismail, S. Ragab, A. El Nemr, Removal of Acid Yellow 11 dye using novel modified biochar derived from watermelon Peels, Desal. Water Treat., 203 (2020) 403–431.
[29] M.A. El-Nemr, I.M.A. Ismail, N.M. Abdelmonem, A. El Nemr, S. Ragab, Amination of biochar derived from watermelon peel by triethylenetetramine and ammonium hydroxide for toxic chromium removal enhancement, Chin. J. Chem. Eng., 36 (2021) 199–222.
[30] J. Goel, K. Kadirvelu, C. Rajagopal, V.K. Garg, Removal of lead(II) by adsorption using treated granular activated carbon: batch and column studies, J. Hazard. Mater. B, 125 (2005) 211–220.
[31] G. Issabayeva, M.K. Aroua, N.M.N. Sulaiman, Removal of lead from aqueous solutions on palm shell activated carbon, Bioresour. Technol., 97 (2006) 2350–2355.
[32] Q. Shi, A. Terracciano, Y. Zhao, C. Wei, C. Christodoulatos, X. Meng, Evaluation of metal oxides and activated carbon for lead removal: kinetics, isotherms, column tests, and the role of co-existing ions, Sci. Total Environ., 648 (2019) 176–183.
[33] M. Inyang, B. Gao, Y. Yao, Y. Xue, A.R. Zimmerman, P. Pullammanappallil, X. Cao, Removal of heavy metals from aqueous solution by biochars derived from anaerobically digested biomass, Bioresour. Technol., 110 (2012) 50–56.
[34] X. Tan, Y. Liu, G. Zeng, X. Wang, X. Hua, Y. Gu, Z. Yang, Application of biochar for the removal of pollutants from aqueous solutions, Chemosphere, 125 (2015) 70–85.
[35] Z. Shen, D. Hou, F. Jin, J. Shi, X. Fan, D.C.W. Tsang, D.S. Alessi, Effect of production temperature on lead removal mechanisms by rice straw biochars, Sci. Total Environ., 655 (2019) 751–758.

[36] A. El Nemr, A.G.M. Shoaib, A. El Sikaily, A.E.-D.A. Mohamed, A.F. Hassan, Evaluation of cationic Methylene blue dye removal by high surface area mesoporous nano activated carbon derived from *Ulva lactuca*, Environ. Process., 8 (2021) 311–332.
[37] A. El Nemr, R.M. Aboughaly, A. El Sikaily, S. Ragab, M.S. Masoud, M.S. Ramadan, Microporous nano-activated carbon type I derived from orange peel and its application for Cr(VI) removal from aquatic environment, Biomass Convers. Biorefin., (2020), doi: 10.1007/s13399-020-00995-5 (in Press).
[38] A.G.M. Shoaib, A. El-Sikaily, A. El Nemr, A.E.-D.A. Mohamed, A.A. Hassan, Preparation and characterization of highly surface area activated carbons followed Type IV from marine red alga (*Pterocladia capillacea*) by zinc chloride activation, Biomass Convers. Biorefin., (2020), doi: 10.1007/s13399-020-00760-8 (in Press).
[39] A.G.M. Shoaib, A. El-Sikaily, A. El Nemr, A.E.-D.A. Mohamed, A.A. Hassan, Testing the carbonization condition for high surface area preparation of activated carbon followed Type IV from green alga *Ulva lactuca*, Biomass Convers. Biorefin., (2020), doi: 10.1007/s13399-020-00823-w (in Press).
[40] T.M. Huggins, A. Haeger, J.C. Biffinger, Z.J. Ren, Granular biochar compared with activated carbon for wastewater treatment and resource recovery, Water Res., 94 (2016) 225–232.
[41] A. El Nemr, R.M. Aboughaly, A. El Sikaily, S. Ragab, M.S. Masoud, M.S. Ramadan, Utilization of sugarcane bagasse/$ZnCl_2$ for sustainable production of microporous nano activated carbons of type I for toxic Cr(VI) removal from aqueous environment, Biomass Convers. Biorefin., (2021), doi: 10.1007/s13399-021-01445-6 (in Press).
[42] T. Sahlabji, M.A. El-Nemr, A. El Nemr, S. Ragab, M.M. Alghamdi, A.A. El-Zahhar, A.M. Idris, T.O. Said, High surface area microporous activated carbon from *Pisum sativum* peels for hexavalent chromium removal from aquatic environment, Toxin Rev., (2021), doi: 10.1080/15569543.2021.1908361 (in Press).
[43] M. Uchimiya, L.H. Wartelle, K.T. Klasson, C.A. Fortier, I.M. Lima, Influence of pyrolysis temperature on biochar property and function as a heavy metal sorbent in soil, J. Agric. Food Chem., 59 (2011) 2501–2510.
[44] C. Chen, H. Liu, T. Chen, An insight into the removal of Pb(II), Cu(II), Co(II), Cd(II), Zn(II), Ag(I), Hg(I), Cr(VI) by Na(I)-montmorillonite and Ca(II)-montmorillonite, Appl. Clay Sci., 118 (2015) 239–247.
[45] T. Chen, Z. Zhou, R. Han, R. Meng, H. Wang, W. Lu, Adsorption of cadmium by biochar derived from municipal sewage sludge: impact factors and adsorption mechanism, Chemosphere, 134 (2015) 286–293.
[46] D. Chen, Z. Zheng, K. Fu, Z. Zeng, J. Wang, M. Lu, Torrefaction of biomass stalk and its effect on the yield and quality of pyrolysis products, Fuel, 159 (2015) 27–32.
[47] Y. Shen, Chars as carbonaceous adsorbents/catalysts for tar elimination during biomass pyrolysis or gasification, Renewable Sustainable Energy Rev., 43 (2015) 281–295.
[48] L. Wang, Y. Wang, F. Ma, V. Tankpa, S. Bai, X. Guo, X. Wang, Mechanisms and reutilization of modified biochar used for removal of heavy metals from wastewater: a review, Sci. Total Environ., 668 (2019) 1298–1309.
[49] M. Kobya, E. Demirbas, E. Senturk, M. Ince, Adsorption of heavy metal ions from aqueous solutions by activated carbon prepared from apricot stone, Bioresour. Technol., 96 (2005) 1518–1521.
[50] I. Kula, M. Uğurlu, H. Karaoğlu, A. Çelik, Adsorption of Cd(II) ions from aqueous solutions using activated carbon prepared from olive stone by $ZnCl_2$ activation, Bioresour. Technol., 99 (2008) 492–501.
[51] T. Budinova, N. Petrov, J. Parra, V. Baloutzov, Use of an activated carbon from antibiotic waste for the removal of Hg(II) from aqueous solution, J. Environ. Manage., 88 (2008) 165–172.
[52] Y. Sudaryanto, S.B. Hartono, W. Irawaty, H. Hindarso, S. Ismadji, High surface area activated carbon prepared from cassava peel by chemical activation, Bioresour. Technol., 97 (2006) 734–739.
[53] D. Borah, S. Satokawa, S. Kato, T. Kojima, Sorption of As(V) from aqueous solution using acid modified carbon black, J. Hazard. Mater., 162 (2009) 1269–1277.
[54] A. Reffas, V. Bernardet, B. David, L. Reinert, M.B. Lehocine, M. Dubois, N. Batisse, L. Duclaux, Carbons prepared from coffee grounds by H_3PO_4 activation: characterization and adsorption of methylene blue and Nylosan Red N-2RBL, J. Hazard. Mater., 175 (2010) 779–788.
[55] P.D. Pathak, S.A. Mandavgane, B.D. Kulkarni, Characterizing fruit and vegetable peels as bioadsorbents, Curr. Sci., 110 (2016) 2114–2124.
[56] N. Feng, X. Guo, S. Liang, Y. Zhu, J. Liu, Biosorption of heavy metals from aqueous solutions by chemically modified orange peel, J. Hazard. Mater., 185 (2011) 49–54.
[57] J.R. Memon, S.Q. Memon, M.I. Bhanger, A. El-Turki, K.R. Hallam, G.C. Allen, Banana peel: a green and economical sorbent for the selective removal of Cr(VI) from industrial wastewater, Colloids Surf., B, 70 (2009) 232–237.
[58] S. Schiewer, S.B. Patil, Modeling the effect of pH on biosorption of heavy metals by citrus peels, J. Hazard. Mater., 157 (2008) 8–17.
[59] M. Iqbal, A. Saeed, S.I. Zafar, FTIR spectrophotometry, kinetics and adsorption isotherms modeling, ion exchange, and EDX analysis for understanding the mechanism of Cd^{2+} and Pb^{2+} removal by mango peel waste, J. Hazard. Mater., 164 (2009) 161–171.
[60] K.H. Chong, B. Volesky, Description of two-metal biosorption equilibria by Langmuir-type models, Biotechnol. Bioeng., 47 (1995) 451–460.
[61] S.J. Gregg, K.S.W. Sing, Adsorption Surface Area and Porosity, 2nd ed., Academic Press Inc., London, 1982.
[62] F. Rouquerol, J. Rouquerol, K.S.W. Sing, Adsorption by Powders and Porous Solids, Academic Press Inc., London, 1999.
[63] E.P. Barrett, L.G. Joyner, P.P. Halenda, The determination of pore volume and area distributions in porous substances. I. Computations from nitrogen isotherms, J. Am. Chem. Soc., 73 (1951) 373–380.
[64] I. Langmuir, The constitution and fundamental properties of solids and liquids, J. Am. Chem. Soc., 38 (1916) 2221–2295.
[65] M. Doğan, M. Alkan, Y. Onganer, Adsorption of methylene blue from aqueous solution onto perlite, Water Air Soil Pollut., 120 (2000) 229–249.
[66] D.G. Kinniburgh, General purpose adsorption isotherms, Environ. Sci. Technol., 20 (1986) 895–904.
[67] E. Longhinotti, F. Pozza, L. Furlan, M.D.N.D. Sanchez, M. Klug, M.C.M. Laranjeira, V.T. Favere, Adsorption of anionic dyes on the biopolymer chitin, J. Braz. Chem. Soc., 9 (1998) 435–440.
[68] A. El Nemr, A. El-Sikaily, A. Khaled, Modeling of adsorption isotherms of Methylene blue onto rice husk activated carbon, Egypt. J. Aquat. Res., 36 (2010) 403–425.
[69] H.M.F. Freundlich, Über die adsorption inlösungen, Z. Phys. Chem. (Leipzig), 57A (1906) 385–470.
[70] M.J. Temkin, V. Pyzhev, Kinetics of ammonia synthesis on promoted iron catalysts, Acta Physiochim, URSS, 12 (1940) 217–222.
[71] D. Kavitha, C. Namasivayam, Experimental and kinetic studies on methylene blue adsorption by coirpith carbon, Bioresour. Technol., 98 (2007) 14–21.
[72] C. Aharoni, M. Ungarish, Kinetics of activated chemisorption. Part 2. Theoretical models, J. Chem. Soc. Faraday Trans., 73 (1977) 456–464.
[73] C. Aharoni, D.L. Sparks, Kinetics of Soil Chemical Reactions—A Theoretical Treatment, D.L. Sparks, D.L. Suarez, Eds., Rate of Soil Chemical Processes, Soil Sci. Soc. America, Madison, WI, 1991, pp. 1–18.
[74] X.S. Wang, Y. Qin, Equilibrium sorption isotherms for of Cu^{2+} on rice bran, Process Biochem., 40 (2005) 677–680.
[75] C.I. Pearce, J.R. Lioyd, J.T. Guthrie, The removal of color from textile wastewater using whole bacterial cells: a review, Dyes Pigm., 58 (2003) 179–196.
[76] G. Akkaya, A. Özer, Adsorption of Acid Red 274 (AR 274) on *Dicranella varia*: determination of equilibrium and kinetic model parameters, Process Biochem., 40 (2005) 3559–3568.
[77] L.V. Radushkevich, Potential theory of sorption and structure of carbons, Zhurnal Fizicheskoi Khimii, 23 (1949) 1410–1420.
[78] M.M. Dubinin, The potential theory of adsorption of gases and vapors for adsorbents with energetically non-uniform surface, Chem. Rev., 60 (1960) 235–266.

[79] M.M. Dubinin, Modern state of the theory of volume filling of micropore adsorbents during adsorption of gases and steams on carbon adsorbent, Zhurnal Fizicheskoi Khimii, 39 (1965) 1305–1317.
[80] S. Lagergren, Zurtheorie der sogenannten adsorption gelosterstoffe, Kungliga Svenska Vetenskapsakademiens, Handlingar, 24 (1898) 1–39.
[81] Y.S. Ho, G. McKay, D.A.J. Wase, C.F. Foster, Study of the sorption of divalent metal ions on to peat, Adsorpt. Sci. Technol., 18 (2000) 639–650.
[82] J. Zeldowitsch, Über den mechanismus derkatalytischen oxidation von CO and MnO_2, Acta Physicochim. URSS, 1 (1934) 364–449.
[83] S.H. Chien, W.R. Clayton, Application of Elovich equation to the kinetics of phosphate release and sorption on soils, Soil Sci. Soc. Am. J., 44 (1980) 265–268.
[84] D.L. Sparks, Kinetics of Reaction in Pure and Mixed Systems, in Soil Physical Chemistry, CRC Press, Boca Raton, 1986.
[85] W.J. Weber, J.C. Morris, Kinetics of adsorption on carbon from solution, J. Sanit. Eng. Div. Am. Soc. Civ. Eng., 89 (1963) 31–60.
[86] K. Srinivasan, N. Balasubramanian, T.V. Ramakrishan, Studies on chromium removal by rice husk carbon, Ind. J. Environ. Health, 30 (1988) 376–387.
[87] J.F. Porter, G. McKay, K.H. Choy, The prediction of sorption from a binary mixture of acidic des using single-and mixed-isotherm variants of the ideal adsorbed solute theory, Chem. Eng. Sci., 54 (1999) 5863–5885.
[88] S.J. Allen, Q. Gan, R. Matthews, P.A. Johnson, Comparison of optimized isotherm models for basic dye adsorption by kudzu, Bioresour. Technol., 88 (2003) 143–152.
[89] Y.S. Ho, W.T. Chiu, C.C. Wang, Regression analysis for the sorption isotherms of basic dyes on sugarcane dust, Bioresour. Technol., 96 (2005) 1285–1291.
[90] J. Fu, Z. Chen, M. Wang, S. Liu, J. Zhang, J. Zhang, R. Han, Q. Xu, Adsorption of methylene blue by a high-efficiency adsorbent (polydopamine microspheres): kinetics, isotherm, thermodynamics and mechanism analysis, Chem. Eng. J., 259 (2015) 53–61.
[91] S. Chowdhury, S. Chakraborty, P. Saha, Biosorption of Basic Green 4 from aqueous solution by *Ananas comosus* (pineapple) leaf powder, Colloids Surf., B, 84 (2011) 520–527.
[92] E.S. Mobasherpour, M. Pazouki, Comparative of the removal of Pb^{2+}, Cd^{2+} and Ni^{2+} by nano crystallite hydroxyapatite from aqueous solutions: adsorption isotherm study, Arabian J. Chem., 5 (2012) 439–446.
[93] B. Yu, Y. Zhang, A. Shukla, S.S. Shukla, K.L. Dorris, The removal of heavy metals from aqueous solutions by sawdust adsorption—removal of lead and comparison of its adsorption with copper, J. Hazard. Mater. B, 84 (2001) 83–94.
[94] C. Huang, C. Huang, A.L. Morehart, The removal of Cu(II) from dilute aqueous solutions by *Saccharomyces cerevisiae*, Water Res., 24 (1990) 433–439.
[95] G. Annadural, R.S. Juang, D.J. Lee, Adsorption of heavy metals from water using banana and orange peels, Water Sci. Technol., 47 (2003) 185–190.
[96] R. Razmovski, M. Šćiban, Biosorption of Cr(VI) and Cu(II) by waste tea fungal biomass, Ecol. Eng., 34 (2008) 179–186.
[97] J.R. Lujan, D.W. Darnall, P.C. Stark, G.D. Rayson, J.L. Gardea-Torresdey, Metal ion binding by algae and higher plant tissues: a phenomenological study of solution pH dependence, Solvent Extr. Ion Exch., 12 (1994) 803–816.
[98] Y.-S. Ho, Removal of copper ions from aqueous solution by tree fern, Water Res., 37 (2003) 2323–2330.
[99] C. Liu, H.H. Ngo, W. Guo, K.-L. Tung, Optimal conditions for preparation of banana peels, sugarcane bagasse and watermelon rind in removing copper from water, Bioresour. Technol., 119 (2012) 349–354.